Thermodynamic approaches to phases transformations 1– diffusive

Charles-André GANDIN

PSL University, Mines Paris, CEMEF UMR CNRS 7635, Sophia Antipolis, France

Colloque National MECAMAT – Simulation et instrumentation des procédés d'élaboration et de fabrication – 22-26 Janvier 2024, Aussois, FR

Introduction

- Phase transformations
  - Present in our natural environment
  - Present in most of the industrial forming processes of materials that produce objects
  - Define the microstructure of the objects, hence its mechanical and physical properties
  - Key for understanding how
    - to create good quality products
    - to optimize production (energy-efficient routes to cheap products)
  - Involve simulation and instrumentation studies to help controlling the forming routes of the products
  - Closely linked to thermodynamic concepts

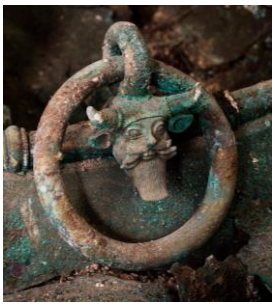

Cauldron cove,
Vth century B.C.,
Lavau (France)
www.inrap.fr/l-age-du-fer-10233

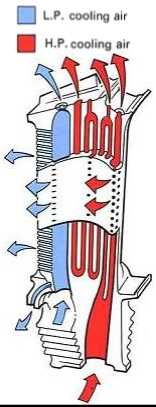

High pressure turbine blade for turbojet engine with serpentine multi-pass multi-feed internal cooling design
aerospaceengineeringblog.com/turbine-cooling

Introduction

- Thermodynamics
  - Study of the behavior of a system of matter under the action of external fields (e.g., temperature T, pressure p)
    - *System* Ω
      Matter that can interact within a space of defined boundary $\partial\Omega$
    - *Components* $i = \{A, B, \ldots\}$
      Chemically distinct entities (e.g., elements)
    - *Phases* $\varphi = \{\alpha, \beta, \ldots\}$
      Portions of a system that are physically distinct in terms of state (e.g., solid, liquid, gas), crystal structure or molar composition of components (e.g., $X_{\beta A} \neq X'_{\beta A}$)
  - Equilibrium
    - The most stable state of the system
    - Thermodynamic equilibrium implies that the transformations of the system take place over a sufficient long period of time to avoid spatial variations in temperature, composition, pressure, etc.

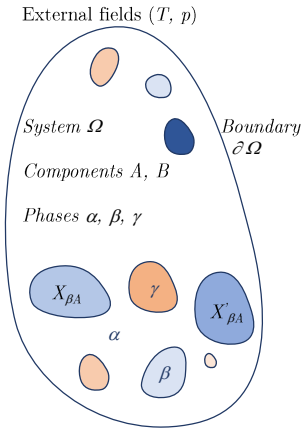

MINES PARIS | PSL | Cemef cnrs

3

Contents

MINES PARIS | PSL | Cemef cnrs

4

Definitions

- Thermodynamic variables
  - ***Extensive*** variable does depend on the quantity of material Volume V, Mass M, Number of moles n, Internal energy E, Gibbs free energy G, Enthalpy H, Entropy S
  - ***Intensive*** variable does not depend on the amount of material Temperature T, Pressure p, Specific quantities $e = E/M$, $g = G/M$, $h = H/M$, $s = S/M$, Molar quantities $E^m = E/n$, $G^m = G/n$, $H^m = H/n$, $S^m = S/n$, $V^m = V/n$
- Laws of thermodynamics
  - ***First*** $dE = \delta Q + \delta W$
    - dE total change of internal energy of a system
    - $\delta W = -\,p\,dV$ work done by external forces assuming only compression/expansion terms
    - $\delta Q = \delta Q_{rev} + \delta Q_{irr}$ heat added to the system, sum of reversible and irreversible parts
  - ***Second*** $\delta Q_{irr} \geq 0$
    - $\delta Q_{irr} = 0$ for a succession of steps close to equilibrium states, i.e. a reversible path
    - $dS = \delta Q_{rev}\,/\,T$ defines the entropy S for a reversible path
  - $dE = \delta Q + \delta W = T\,dS - p\,dV$ at equilibrium, E is minimum and S is maximum

MINES PARIS | PSL | Cemef cnrs

Enthalpy and Gibbs free energy

- Enthalpy: $H = E + p\,V$
  - $dH = dE + p\,dV + V\,dp = T\,dS + V\,dp$
  - Dividing by the constant mass M of the system, $h = H(T,p)/M$ $c_p = (\partial h/\partial T)_p$ defines the ***specific heat at constant pressure*** (can be measured by calorimetry)
  - It follows $ds = (dh/T)_p = (c_p\,dT/T)_p$, hence $s(T) = \int_{0K}^{T} \frac{c_p(\theta)}{\theta} d\theta$ defines the entropy of the system at T
  - By convention, the entropy is zero at absolute zero
- Gibbs free energy: $G = H - T\,S$
  - $dG = dH - S\,dT - T\,dS = V\,dp - S\,dT$
  - $G = G(p,T)$ is the state variable that is naturally dependent on the intensive variables p and T
  - $S = -(\partial G/\partial T)_p$ gives access to the ***entropy of the system***
  - At constant pressure, G necessary decreases when increasing T

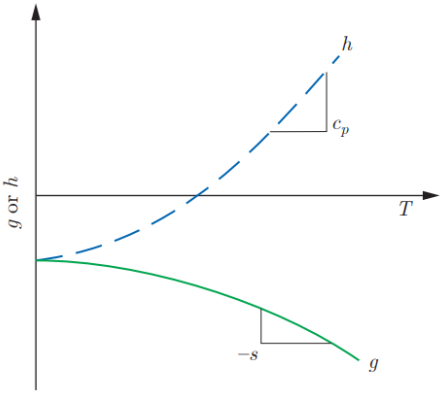

Specific enthalpy and Gibbs free energy per unit mass as a function of temperature for a constant pressure p (Dantzig and Rappaz, Solidification (2016) EPFL Press)

MINES PARIS | PSL | Cemef cnrs

Unary multiple phase system

- Gibbs free energy of a two-phase system, α and β
  - $G^m = \chi_\alpha G^m_\alpha + \chi_\beta G^m_\beta$ $\quad G^m_\alpha, G^m_\beta$ Gibbs free energy of phase α and β
    χ_α, χ_β mole fraction of phase α and β with $\chi_\alpha + \chi_\beta = 1$
- Condition for a minimum energy of the system at equilibrium
  - $\frac{\partial G^m}{\partial \chi_\alpha} = G^m_\alpha - G^m_\beta = 0 \quad G^m_\alpha = G^m_\beta = G^m$
  - $dG = V\,dp - S\,dT$ At equilibrium, a unary two-phase system satisfies $p_\alpha = p_\beta$ and $T_\alpha = T_\beta$
- Interpretations (for solidification)
  - T_f Equilibrium temperature between solid and liquid
  - $S^m_s < S^m_l$ The liquid is more disordered than the solid
  - $\Delta S^m_f = S^m_l - S^m_s$ Molar entropy of fusion $\Delta S^m_f = L^m_f / T_f$ with $L^m_f = H^m_l(T_f) - H^m_s(T_f)$ the molar enthalpy of fusion (or latent heat of fusion per mole) established at equilibrium with $G^m_l = G^m_s$ at T_f

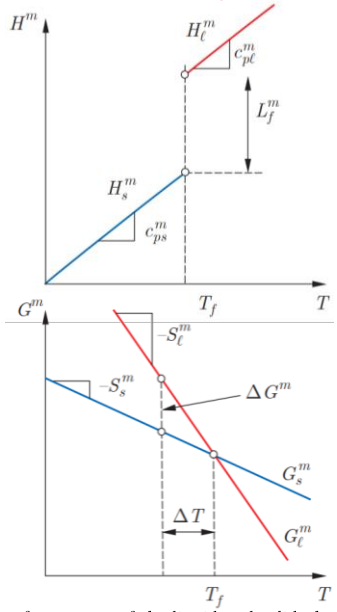

Molar enthalpy and molar free energy of the liquid and solid phases of a unary system as a function of temperature for a constant pressure p (Dantzig and Rappaz, Solidification (2016) EPFL Press)

Unary multiple phase system (cont'd)

- Equilibrium phase diagram
  - Defines the domains of existence of phases as a function of pressure and temperature
  - For a given pressure and temperature, the stable phase is defined by the lowest value of the Gibbs free energy
  - For water, at pressure $p_a = 1013.25$ hPa
    - melting temperature (ice → liquid) $T_f = 0°$ C,
    - vaporization temperature (liquid → gas) $T_v = 100°$ C
  - At pressure p_t
    - 3 phases coexist, named triple point, where the pressure and the temperature are fixed
  - Lines of phase diagram where 2 phases coexist are monovariant lines. Pressure and temperature are no longer independent.

Equilibrium phase diagram for water and schematics Gibbs free energies at atmospheric pressure p_a (dashed curves) and at the triple point pressure p_t (solid lines) (Dantzig and Rappaz, Solidification (2016) EPFL Press)

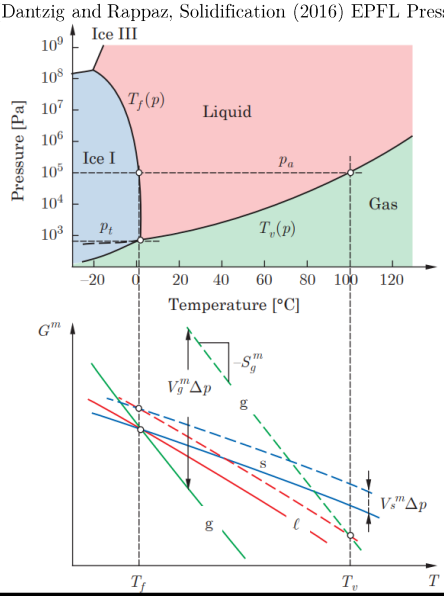

Unary multiple phase system (cont'd)

- Consequence on thermal history of a water sample cooled at atmospheric pressure from the gas state ($T > T_v$) with a constant heat extraction rate, $(dh/dt) < 0$.
  - The cooling rate, (dT/dt), is proportional to $(dh/dt)/c_p$ (specific heat $c_{pl} = 4.18$ J g^{-1} K^{-1})
    - with $c_{pg} = c_{ps}$, $(dT/dt)_g = (dT/dt)_s$,
    - with $c_{pl} = 2\ c_{pg}$, $(dT/dt)_l = (1/2)\ (dT/dt)_s$.
  - The length of the temperature plateaus is proportional to the time of
    - condensation at p_a and $T_v = 100$ °C with latent heat $L_v = 2250$ J g^{-1} ,
    - solidification at p_a and $T_f = 0°$ C with latent heat $L_f = 333$ J g^{-1} .

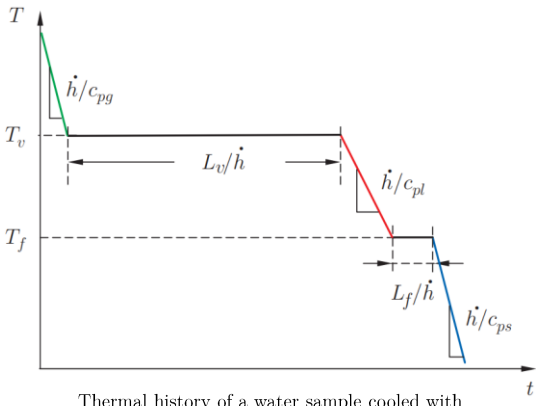

Thermal history of a water sample cooled with a constant heat extraction rate,$(\frac{dh}{dt} = \dot{h}) < 0$, at atmosphere pressure. (Dantzig and Rappaz, Solidification (2016) EPFL Press)

MINES PARIS | PSL | Cemef cnrs

Binary single phase system

- Let's consider a single phase made of two components A and B, with A the major component and B the minor component
  - A is called the ***solvent***, B is called the ***solute***
  - ***Compositions*** in mole fraction are $X_A = n_A/(n_A+n_B)$ and $X_B = n_B/(n_A+n_B)$, with $X_A + X_B = 1$
  - The differential form of the Gibbs free energy of the system, $G = G(p,T,n_A,n_B)$, becomes

(eq. 1) $$dG(p,T,n_A,n_B) = V(p,T,n_A,n_B)\ dp - S(p,T,n_A,n_B)\ dT + \mu_A(p,T,X_B)\ dn_A + \mu_B(p,T,X_B)\ dn_B$$

where $\boldsymbol{\mu_A} = (\partial G/\partial n_A)_{p,T,n_B}$ and $\boldsymbol{\mu_B} = (\partial G/\partial n_B)_{p,T,n_A}$ are the ***chemical potentials*** of each component. Using the definition of the molar compositions leads to the differential form of the ***molar Gibbs free energy of the system***

$$dG^m(p,T,X_B) = V^m(p,T,X_B)dp - S^m(p,T,X_B)dT + [\mu_B(p,T,X_B) - \mu_A(p,T,X_B)]dX_B$$

  - At fixed temperature and pressure, the Gibbs free energy writes *(eq. 2)* $G = n_A\ \mu_A + n_B\ \mu_B$ leading to $dG = n_A\ d\mu_A + n_B\ d\mu_B + \mu_A\ dn_A + \mu_B\ dn_B$. Equating with *(eq. 1)* leads to the Gibbs-Duhem equation $n_A\ d\mu_A + n_B\ d\mu_B = 0$.

MINES PARIS | PSL | Cemef cnrs

Binary single phase system (cont'd)

Thermodynamics

- In the molar form, *(eq. 2)* becomes *(eq. 3)* $G^m = X_A\,\mu_A + X_B\,\mu_B$ and the Gibbs-Duhem equation becomes $X_A\,d\mu_A + X_B\,d\mu_B = 0$. *(eq. 3)* and its differentiated form lead to

$$\mu_A(p,T,X_B) = G^m(p,T,X_B) - X_B\,(\partial G^m/\partial X_B)_{p,T}$$
$$\mu_B(p,T,X_B) = G^m(p,T,X_B) + (1\text{-}X_B)\,(\partial G^m/\partial X_B)_{p,T}$$

- The chemical potentials of components A and B of the system of composition X_B at constant pressure and temperature can be determined by the geometric construction called ***tangent rule***: the tangent to $G^m(p,T,X_B)$ at X_B intersects the axis $X_A = 1$ (or $X_B = 0$) at $\mu_A(p,T,X_B)$ and the axis $X_B = 1$ at $\mu_B(p,T,X_B)$.

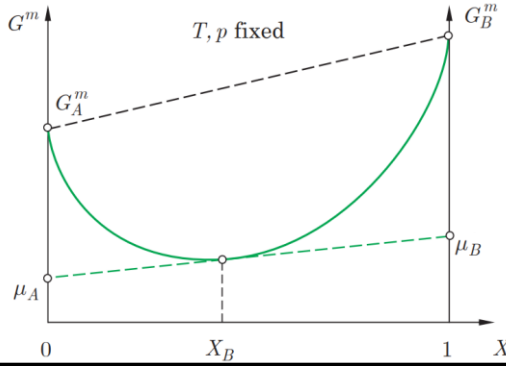

Molar free energy of a binary solution as a function of the mole fraction of component B, showing the tangent construction to compute the chemical potentials μ_A and μ_B, at constant temperature T and pressure p (Dantzig and Rappaz, Solidification (2016) EPFL Press)

MINES PARIS | PSL | Cemef cnrs

11

Binary single phase system (cont'd)

Thermodynamics

- Internal energy of a mixture of components A and B
  - Enthalpy of mixing

    $\Delta H_{mix} = \Omega^m X_A X_B$

    with Ω^m proportional to the excess of energy of A-B bonds
  - Entropy of mixing, $S_{mix}{}^m$, proportional to the vibrational energy due to the mixing of atoms A and B. It follows the number of distinguishable configurations for N_A A-atoms and N_B B-atoms (with $N_A + N_B = N_0$)

    $S_{mix}{}^m = k_B \ln[\,(N_A + N_B)!\,/\,(N_A!\,N_B!)\,]$
  - General form of the molar free energy (***regular solution***) ($\ln x! \approx x \ln x - x$ for $x \to \infty$ and $R = k_B N_0$):

    $G^m = X_A G_A{}^m + X_B G_B{}^m + \Omega^m X_A X_B + RT(X_A \ln X_A + X_B \ln X_B)$

    where $G_J{}^m = E_j{}^m + pV_J{}^m - TS_J{}^m$ $(J{=}A,B)$
  - With $\Omega^m = 0$ (same bonding for between atoms A-B, A-A and B-B), retrieves the ***ideal solution*** approximation

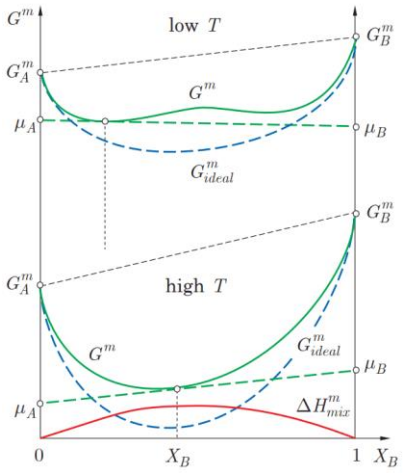

Contributions to the molar free energy of a binary solution as a function of the mole fraction of component B for a regular solution with $\Omega^m > 0$, at low and high temperature T and constant pression p (Dantzig and Rappaz, Solidification (2016) EPFL Press)

MINES PARIS | PSL | Cemef cnrs

12

Binary multiple phase system

Thermodynamics

- Let's consider a two-phase system, s and l, made of components A and B with composition X_{B0}
- At $G_l^m = G_s^m$ and $X_{Bs} = X_{Bl} = X_{B0}$

  $\mu_{As} \neq \mu_{Al}$ and $\mu_{Bs} \neq \mu_{Bl}$. The system can evolve to transfer atoms A from liquid to solid and atoms B from solid to liquid. The associated variation of energy would be $dG = (\mu_{As} - \mu_{Al})\ dn_A + (\mu_{Bl} - \mu_{Bs})\ dn_B < 0$.
  $dG \neq 0$ is not equilibrium!
- Condition for equilibrium: $\mu_{As} = \mu_{Al}$ and $\mu_{Bs} = \mu_{Bl}$

  This is reached at composition X_{Bs} and X_{Bl}, where a ***common tangent*** is found for the molar Gibbs free energy curves of both the solid and liquid phases. Phases s and l coexist in the range $X_{Bs} < X_{B0} < X_{Bl}$.

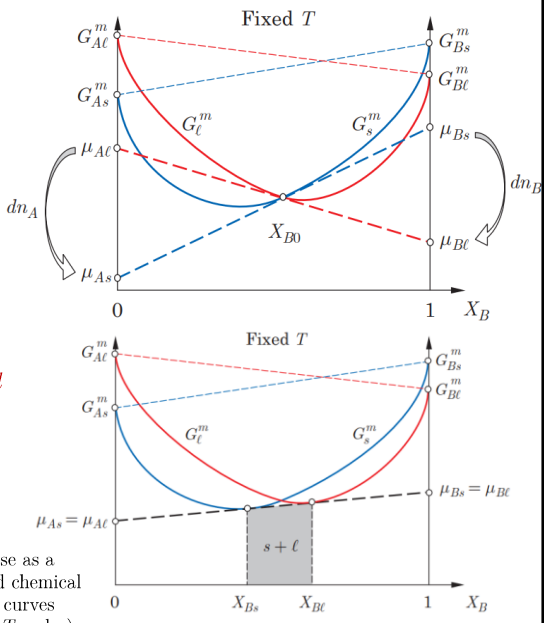

Molar free energies of a solid and a liquid phase as a function of the mole fraction of component B and chemical potentials (top) at the intersection of the two curves (bottom) using the common tangent rule (fixed T and p) (Dantzig and Rappaz, Solidification (2016) EPFL Press)

MINES PARIS | PSL | Cemef | cnrs

13

Binary multiple phase system (cont'd)

Thermodynamics

- Solute conservation
  - At equilibrium, phase composition is uniform, given by the common tangent construction. The phase fractions are deduced from solute conservation for alloy of composition X_{B0}

$$X_{B0} = \chi_s\, X_{Bs} + \chi_l\, X_{Bl} \quad \text{with} \quad \chi_s + \chi_l = 1$$

$$\text{leading to} \quad \chi_s = (X_{Bl} - X_{B0}) \,/\, (X_{Bl} - X_{Bs})$$

$$\chi_l = (X_{B0} - X_{Bs}) \,/\, (X_{Bl} - X_{Bs})$$

  These expressions are known as ***(inverse) lever rule.***
  - The **partition coefficient** is defined by the ratio $k_0 = X_{Bs}/X_{Bl}$
- Equilibrium phase diagram
  - The graph $T(X_B)$ is named **equilibrium phase diagram**
  - Boundaries between regions of the phase diagram define
    - the **solidus temperature,** $T_{sol}(X_B)$, between regions s and $s+l$
    - the **liquidus temperature,** $T_{liq}(X_B)$, between regions l and $s+l$
  - The T_0 **temperature,** $T_0(X_B)$, is defined for $G_l^m = G_s^m$

Phase diagram showing the domain of existence of the liquid and solid phases as a function of temperature and mole fraction of component B (fixed p) (Dantzig and Rappaz, Solidification (2016) EPFL Press)

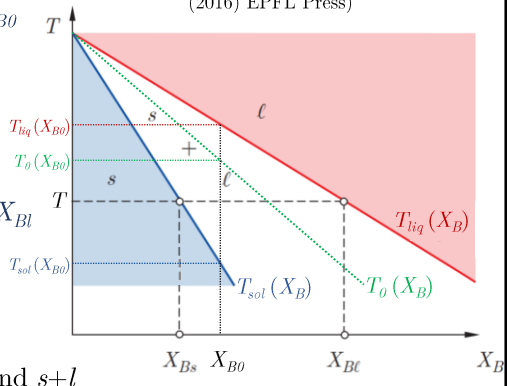

MINES PARIS | PSL | Cemef | cnrs

14

Gibbs' phase rule

- Let's consider a close system defined by
  - N_c components (A, B, …)
  - N_φ phases (α, β, …)
  - T the temperature,
  - p the pressure
- Number of free (independent) variables, or variance of the system

$$N_F = N_C - N_\varphi + 2$$

- Definitions
  - $N_F = 1$ Monovariant transformation / lines
  - $N_F = 0$ Invariant transformation / temperature

Phase diagram showing the domain of existence of the liquid and solid phases as a function of temperature and mole fraction of component B (fixed p) (Dantzig and Rappaz, Solidification (2016) EPFL Press)

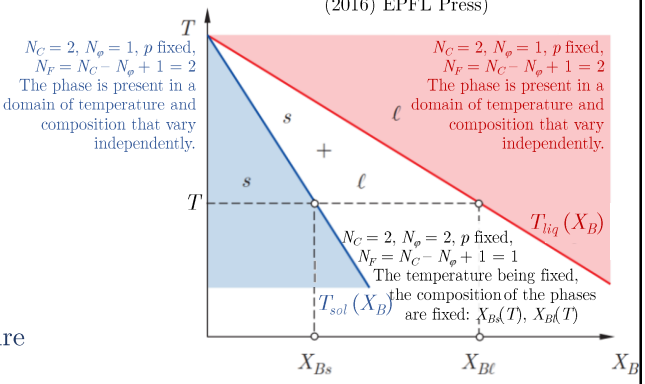

MINES PARIS | PSL | Cemef | cnrs

Binary multiple phase system (cont'd)

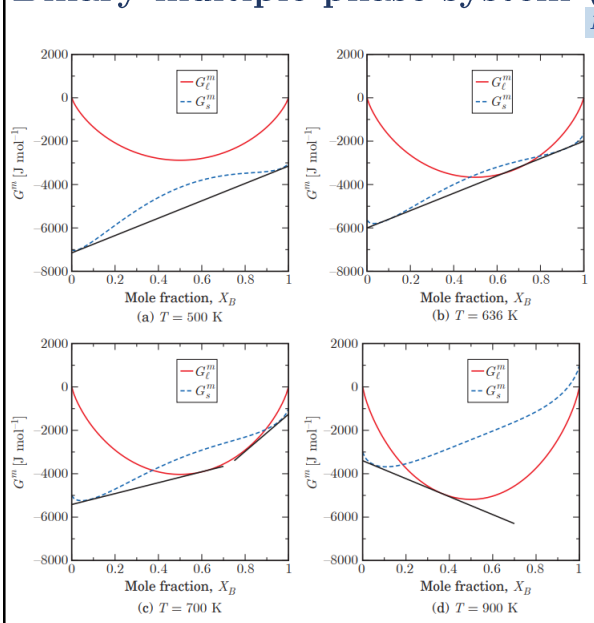

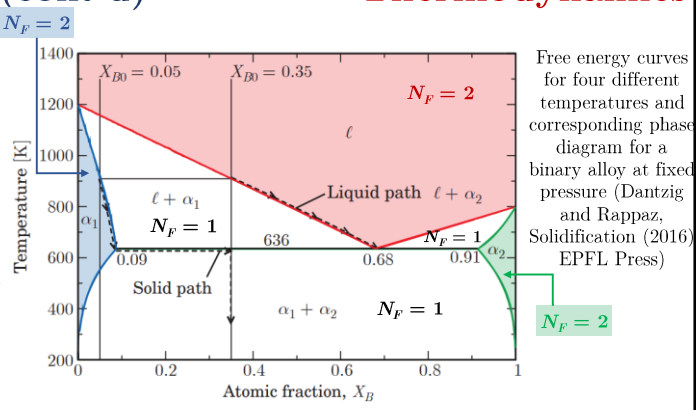

Free energy curves for four different temperatures and corresponding phase diagram for a binary alloy at fixed pressure (Dantzig and Rappaz, Solidification (2016) EPFL Press)

- The horizontal line correspond to the existence of 3 phases in equilibrium at a given T and pressure p
  - $N_C = 2$, $N_\varphi = 3$ (e.g., $\alpha_1 + \alpha_2 + l$), fixed p, $N_F = N_C - N_\varphi + 1 = 0$
  - An *invariant point* exists where 3 phases coexist for given T and X of the phases, corresponding to a "eutectic" transformation.

MINES PARIS | PSL | Cemef | cnrs

Binary multiple phase system (cont'd)

- Invariant reactions
  - Eutectic $l \rightarrow \alpha + \beta$
  - Peritectic $l + \alpha \rightarrow \beta$
  - Monotectic $l_1 \rightarrow l_2 + \alpha$
  - Syntectic $l_1 + l_2 \rightarrow \alpha$
  - Congruent $l \rightarrow \alpha$
  - Spinodal $\alpha \rightarrow \alpha_1 + \alpha_2$
  - Eutectoid $\gamma \rightarrow \alpha + \beta$
  - Peritectoid $\gamma + \alpha \rightarrow \beta$

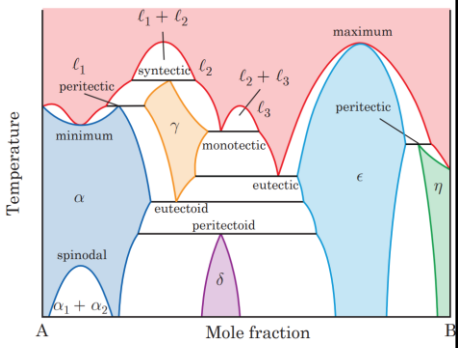

Hypothetical diagram displaying possible invariant reactions in a binary alloy system (Dantzig and Rappaz, Solidification (2016) EPFL Press)

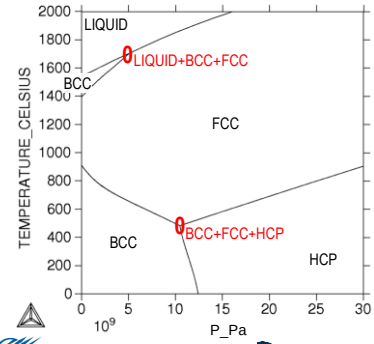

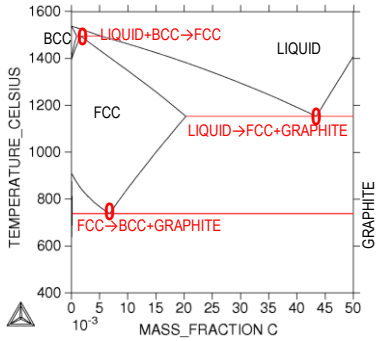

Unary Fe and binary Fe – C phase diagram at p_o with invariant reactions (Thermo-Calc software calculations, TCFE10 thermodynamic database)

Binary multiple phase system (cont'd)

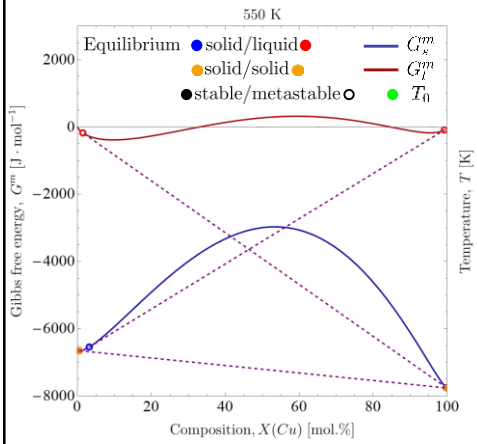

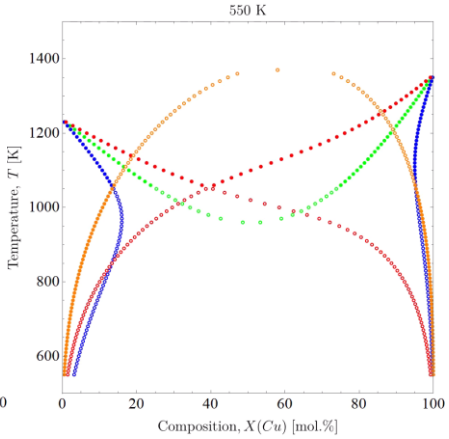

- Stable and metastable phase diagram boundaries are computed for the Ag – Cu system
- Expression of the Gibbs free energies are provided by Murray

Construction of (center) stable and metastable phase diagram boundaries for the Ag – Cu system from (left) the Gibbs free energy curves.
(red symbols) liquidus, (blue symbols) solidus, (green symbols) T_0, (orange symbols) solvus.

$$G_m^\phi = G_{Ag}^{0,\phi} X_{Ag} + G_{Cu}^{0,\phi} X_{Cu}^\phi + RT\left[X_{Ag}^\phi \ln\left(X_{Ag}^\phi\right) + X_{Cu}^\phi \ln\left(X_{Cu}^\phi\right)\right] + f^\phi X_{Ag}^\phi X_{Cu}^\phi + g^\phi X_{Ag}^\phi X_{Cu}^\phi (X_{Ag}^\phi - X_{Cu}^\phi)$$

ϕ	Liquid	Solid (FCC)
G_{Ag}^0	0	$-11945 + 9.67\,T$
G_{Cu}^0	0	$-13054 + 9.62\,T$
f	$15171 - 2.537\,T$	$34532 - 9.178\,T$
g	$-2425 + 0.946\,T$	$-5996 + 1.725\,T$

Murray, metallurgical transactions 15A (1984) 261, animation provided by Gildas Guillemot

Phase transformations with local equilibrium — Example #1

- Small Sn – Pb ingot experiment
  - Left-hand-side (**LHS**) and right-hand-side (**RHS**) heat exchangers with independent control of the time evolution of the temperature
  - 100 x 60 x 10 mm^3 geometry
  - Sn - 3 wt% Pb alloy
  - Temperature history
    - Melting
    - $T_{LHS} - T_{RHS} = 40$ °C
    - Cooling rate = – 0.03 °C/s
  - Thermocouples

    10 columns, 5 rows
  - Positions studied from LHS

    L21 **L24** **L27** **L30**

    5 **35** **65** **95** mm

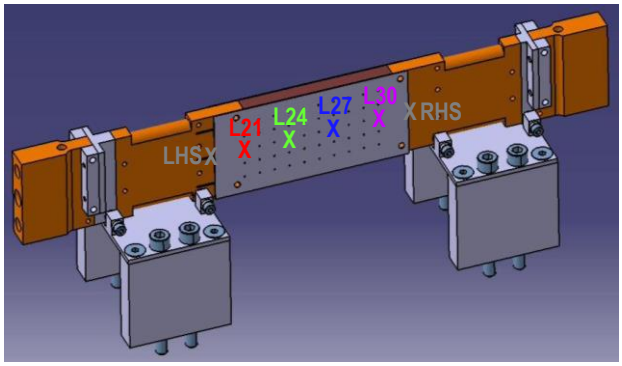

Experiment "Afrodite" developed at Grenoble INP–UGA, SIMAP/EPM, FR

MINES PARIS | PSL | Cemef | cnrs

Hebditch and Hunt, Metallurgical transactions 5 (1974) 1557
Hachani et al., International journal of heat and mass transfer 55 (2012) 1986

19

Experimental data — Example #1

- Recorded temperature histories with thermocouples

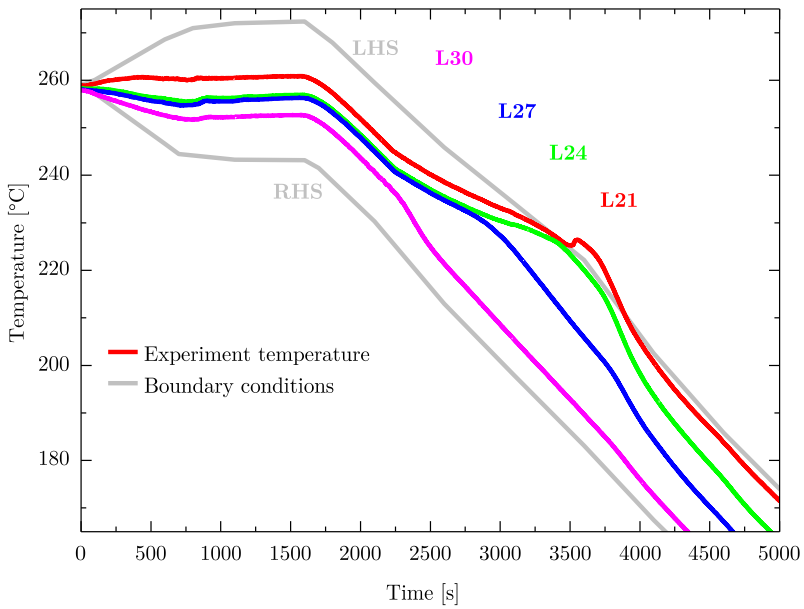

MINES PARIS | PSL | Cemef | cnrs

20

Experimental data

Example #1

- Measured composition map

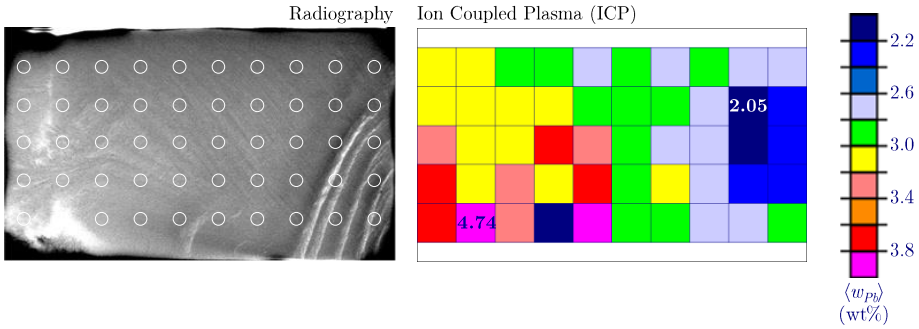

MINES PARIS | PSL | Cemef | cnrs

Thermal and solutal hydraulic flow problem

Example #1

- Finite element solution of the volume-averaged conservation equations
  - Hypotheses: fixed solid ($v^s = 0$), incompressible system ($\rho^s = \rho^l = \rho_0$), no diffusion in solid (D^s=0)
  - Momentum conservation $\rho_0 \dfrac{\partial \langle \mathbf{v} \rangle}{\partial t} + \dfrac{\rho_0}{g^l} \left(\langle \mathbf{v} \rangle \cdot \nabla \right) \langle \mathbf{v} \rangle = \mu^l \, \nabla^2 \langle \mathbf{v} \rangle - g^l \, \nabla \langle p^l \rangle^l + g^l \, \rho \, \mathbf{g} - \mathbf{M}$

    Volumetric friction force $\mathbf{M} = \left(\mu^l / K \right) \, g^l \, \langle \mathbf{v} \rangle$

    Boussinesq approximation $\rho = \rho_0 \left[1 - \beta_{th} (T - T_0) - \beta_w (\langle w^l \rangle^l - w_0) \right]$
  - Total mass conservation $\nabla \cdot \langle \mathbf{v} \rangle = 0$
  - Solute mass conservation $\dfrac{\partial \langle w \rangle}{\partial t} + \langle \mathbf{v} \rangle \cdot \nabla \langle w^l \rangle^l - \nabla \cdot \left(g^l \, D^l \, \nabla \langle w^l \rangle^l \right) = 0$
  - Energy conservation $\rho_0 \left(\dfrac{\partial \langle h \rangle}{\partial t} + \langle \mathbf{v} \rangle \cdot \nabla \langle h^l \rangle^l \right) - \nabla \cdot \left(\langle \kappa \rangle \nabla T \right) = 0$

g^l : volume fraction of liquid
$\langle p^l \rangle^l$: average pressure in liquid
μ^l : liquid viscosity
K : permeability of the mushy zone
β_{th} : thermal expansion
β_w : solutal expansion
T_0 : reference temperature
w_0 : reference solute mass fraction
$\langle h \rangle$: average enthalpy
$\langle h^l \rangle^l$: average enthalpy of liquid
$\langle \kappa \rangle$: average thermal conductivity
D^l : diffusion coefficient in liquid
$\langle w \rangle$: average solute mass
$\langle \mathbf{v} \rangle = g^l \, \langle \mathbf{v}^l \rangle$: average liquid velocity
$\langle w^l \rangle^l$: average solute mass fraction in liquid

MINES PARIS | PSL | Cemef | cnrs

Rappaz, Bellet, Deville, numerical modeling in materials science an engineering (2010) Springer

Thermal flow problem

Example #1

- Average enthalpy and composition $\langle h \rangle = \sum_{\varphi} g^{\varphi}(\langle w \rangle, T) \ \langle h^{\varphi} \rangle^{\varphi}(\langle w^{\varphi} \rangle^{\varphi}, T)$

  $\langle w \rangle = \sum_{\varphi} g^{\varphi}(\langle w \rangle, T) \ \langle w^{\varphi} \rangle^{\varphi}(\langle w \rangle, T)$

  - $g^{\varphi}(\langle w \rangle, T)$ Phase enthalpy at composition w^{φ} and temperature T
  - $\langle h^{\varphi} \rangle^{\varphi}(\langle w^{\varphi} \rangle^{\varphi}, T)$ Fraction of phase φ for an average composition $\langle w \rangle$ and a temperature T
  - $\langle w^{\varphi} \rangle^{\varphi}(\langle w \rangle, T)$ Composition of phase φ for an average composition $\langle w \rangle$ and a temperature T

- Extraction of $g^{\varphi}(\langle w \rangle, T)$, $\langle h^{\varphi} \rangle^{\varphi}(\langle w^{\varphi} \rangle^{\varphi}, T)$, $\langle w^{\varphi} \rangle^{\varphi}(\langle w \rangle, T)$ from a thermodynamic database assuming equilibrium transformations at local composition $\langle w \rangle$ and temperature T
- Tabulations of $g^{\varphi}(\langle w \rangle, T)$, $\langle h^{\varphi} \rangle^{\varphi}(\langle w^{\varphi} \rangle^{\varphi}, T)$, $\langle w^{\varphi} \rangle^{\varphi}(\langle w \rangle, T)$ over a sufficient wide range of local average composition $\langle w \rangle$, temperature T and phase composition $\langle w^{\varphi} \rangle^{\varphi}$
- Lookup procedure to link the average enthalpy at average composition $\langle w \rangle$ to the temperature T

MINES PARIS | PSL | Cemef | cnrs

Tabulations at equilibrium

Example #1

- Phase diagram

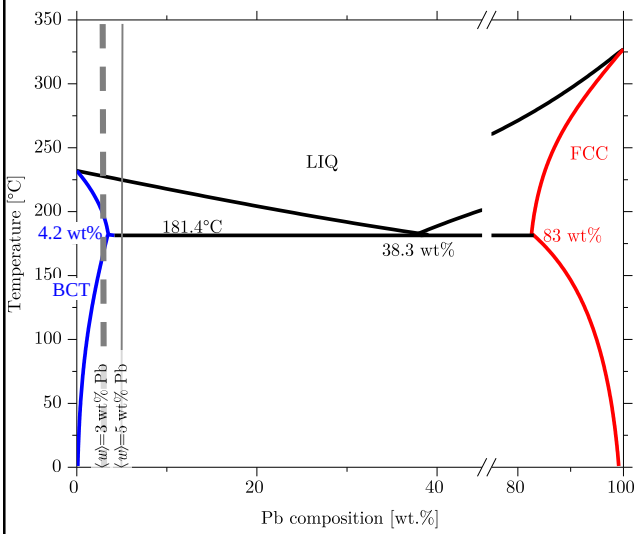

- Transformation paths

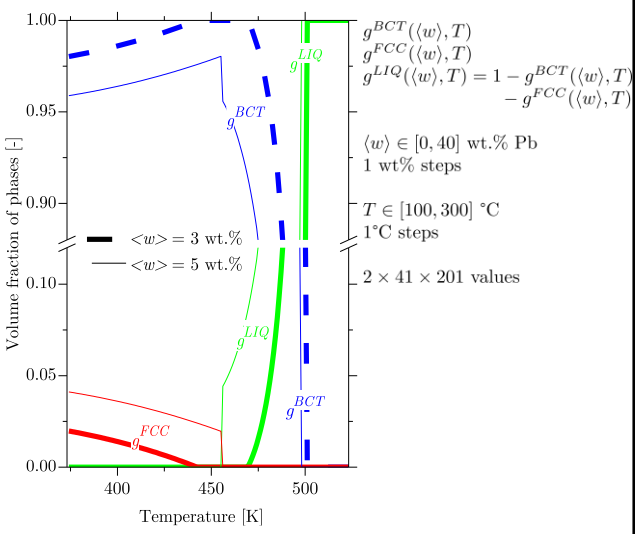

MINES PARIS | PSL | Cemef | cnrs

Sn – Pb equilibrium phase diagram and transformation paths
(Thermo-Calc software calculations, PBIN thermodynamic database)

Tabulations at equilibrium

Example #1

- Phase composition

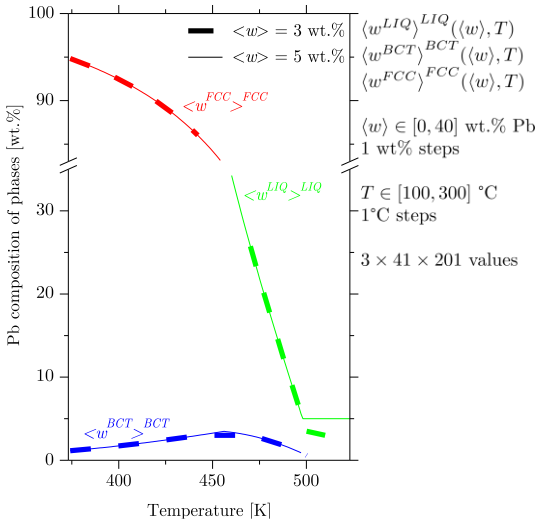

- Phase enthalpy

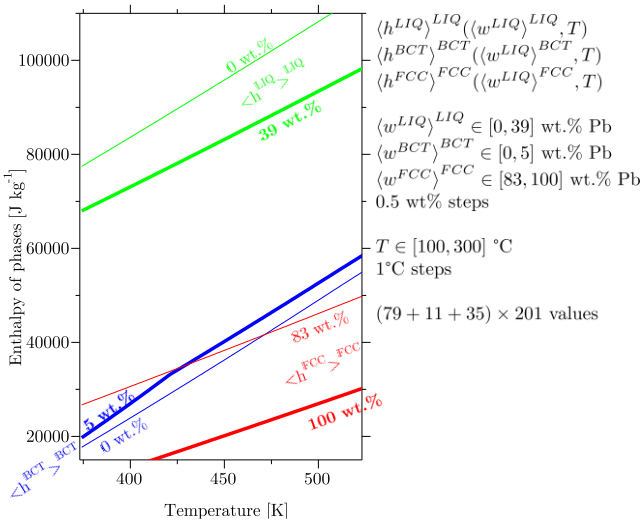

MINES PARIS | PSL | Cemef | cnrs

Sn – Pb phase composition and enthalpy
(Thermo-Calc software calculations, PBIN thermodynamic database)

25

Simulation results

Example #1

- Calculated versus recorded temperature histories

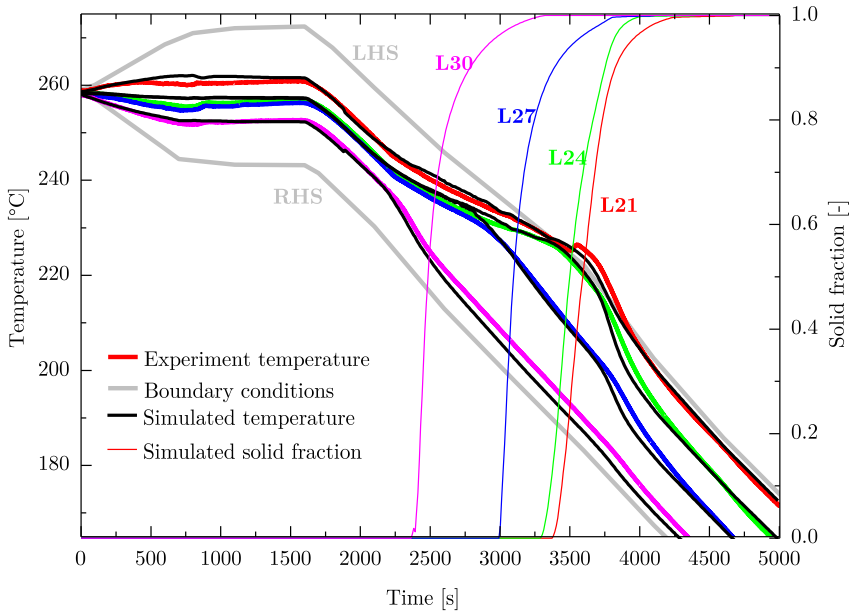

MINES PARIS | PSL | Cemef | cnrs

Carozzani et al., metallurgical and materials transactions 44A (2013) 873

26

Simulation results

Example #1

- Measured composition map

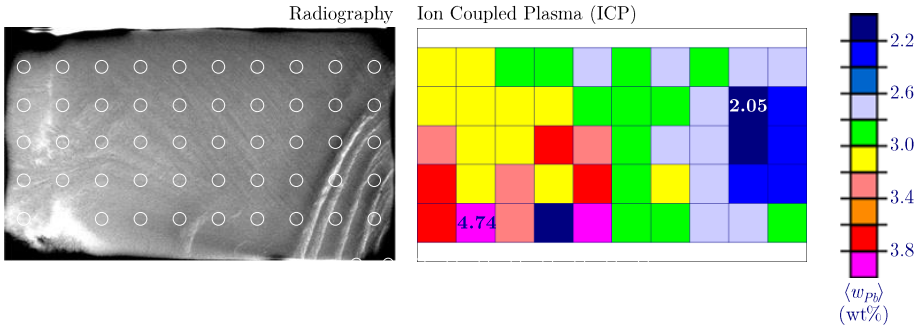

- Calculated composition map

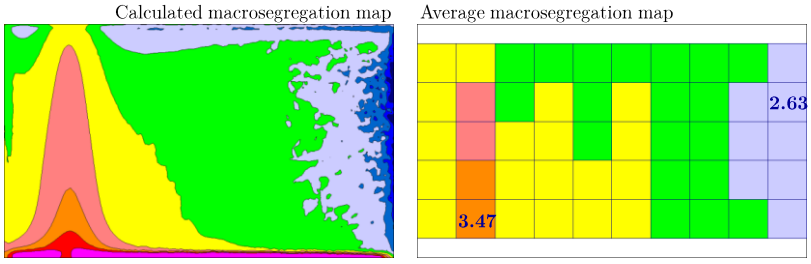

MINES PARIS | PSL | Cemef | cnrs

Carozzani et al., metallurgical and materials transactions 44A (2013) 873 27

Curvature

Diffusional phase transformation

- Unary multiple phase system
  - Excess Gibbs free energy, ΔG_s^m, is present at a curved interface
  - It is induced by the accommodation of structural changes on both sides of the interface
  - Integral of the excess free energy over the thickness of the interface is proportional to the **interfacial energy**, γ_{sl} .
  - For a sphere of radius R and assuming isotropic interfacial energy

$$\Delta G_s^m = V_s^m \ \gamma_{sl} \ 2 \ \bar{\kappa} \quad \text{with the interface curvature} \quad \bar{\kappa} = 1/R$$

  - The Gibbs free energy of the solid phase at equilibrium is increased by ΔG_s^m compared with a planar interface, $G_s^{m\infty}$

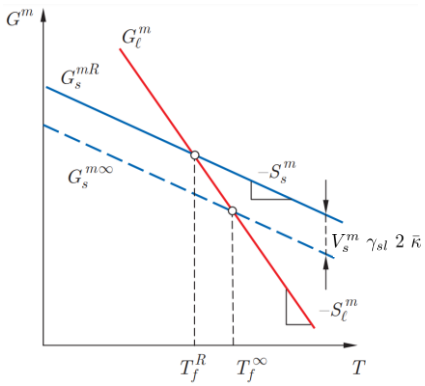

Gibbs free energy for a solid sphere of radius R and the condition of equilibrium with the liquid (Dantzig and Rappaz, Solidification (2016) EPFL Press)

- The associated curvature undercooling ΔT_R is defined by the Gibbs-Thomson coefficient Γ_{sl}

$$\Delta T_R = T_f^\infty - T_f^R = \frac{\Delta G_s^m}{\Delta S_f^m} = 2 \ \Gamma_{sl} \ \bar{\kappa} \quad \text{with} \quad \Gamma_{sl} = \frac{\gamma_{sl} \ V_s^m}{\Delta S_f^m}$$

MINES PARIS | PSL | Cemef | cnrs

28

Curvature (cont'd)

- Binary multiple phase system
  - In alloys, for a spherical particle of radius R, the Gibbs free energy G_s^{mR} is also given by addition of ΔG_s^m to the Gibbs free energy of a planar interface, $G_s^{m\infty}$
  - At a fixed temperature, the **common tangent construction** is applied using G_s^{mR} and G_l^m, leading to **new interface composition at the curved interface**, (X^R_{Bs}, X^R_{Bl}), compared with the equilibrium compositions for a planar interface $(X^\infty_{Bs}, X^\infty_{Bl})$
  - The resulting curvature undercooling is defined by

    $\Delta T_R = 2\,\Gamma_{sl}\,\bar{\kappa}$
  - The equilibrium phase diagram is shift to lower temperatures for all compositions

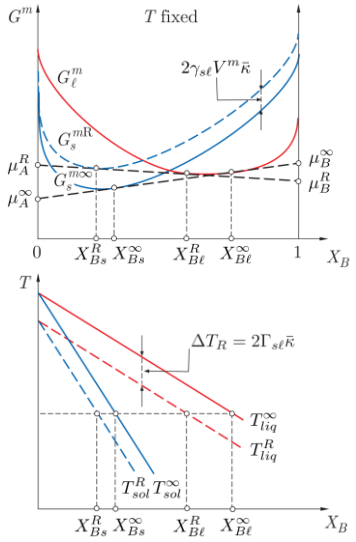

Equilibrium for a binary alloy including the curvature contribution showing (a) shift in free energy curves and (b) shift in the liquidus and solidus curves on the equilibrium phase diagram (Dantzig and Rappaz, Solidification (2016) EPFL Press)

Nucleation

- Homogeneous nucleation
  - Clusters of few atoms present in phase l organize to form embryos of a new phase s. The variation of free energy associated the formation of a cluster is

$$\Delta G = V_s\,\frac{G_s^m - G_l^m}{V^m} + A_{sl}\,\gamma_{sl} \quad \text{with} \quad G_s^m - G_l^m \approx -\Delta S_f^m\,\Delta T$$

$$\Delta G = -\frac{4}{3}\pi R^3\,\rho\Delta s_f\,\Delta T + 4\pi R^2\,\gamma_{sl}$$

  - The nucleus becomes stable if its size exceed the critical radius R_c defined at the maximum of ΔG,

$$\Delta G_n^{homo} = \frac{4\pi\gamma_{sl}R_c^2}{3} = \frac{16\pi}{3}\frac{\gamma_{sl}^3}{(\rho\Delta s_f)^2\Delta T^2} \quad \text{with} \quad R_c = \frac{2\gamma_{sl}}{\rho\Delta s_f\Delta T} = \frac{2\Gamma_{sl}}{\Delta T}$$

  - Assuming a thermally activated process, the nucleation rate is given by

$$I^{homo} = \nu_0 p_c n_l\,\exp\left(-\frac{\Delta G_n^{homo}}{k_B T}\right) = \nu_0 p_c n_l\,\exp\left(-\frac{16\pi}{3}\frac{\gamma_{sl}^3}{(\rho\Delta s_f\Delta T)^2 k_B T}\right)$$

    where n_l is the density of atoms in l and ν_0 is the atomic vibration frequency.

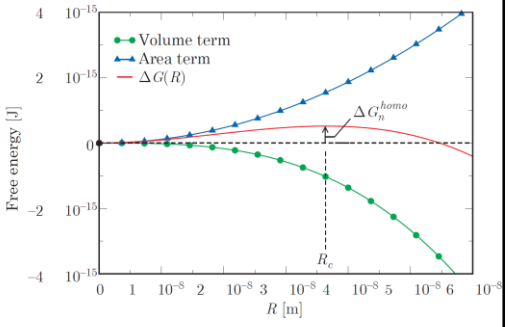

Free energies (surface, bulk and total) of a spherical solid phase of radius R formed in the liquid at a given undercooling (Dantzig and Rappaz, Solidification (2016) EPFL Press)

Nucleation (cont'd)

- Heterogeneous nucleation
  - Nucleation can be initiated on the foreign surface of a particle, a mold, an oxide skin, …, either impurities or intentionally added. The associated variation of free energy is

$$\Delta G = \rho V_s (g_s - g_l) + A_{sl}\gamma_{sl} + A_{fs}(\gamma_{fs} - \gamma_{fl})$$

$$V^s = \frac{\pi R^3}{3}(2+\cos\theta)(1-\cos\theta)^2,\ A_{sl} = 2\pi R^2(1-\cos\theta),\ A_{fs} = \pi R^2(1-\cos^2\theta)$$

$$\Delta G = \left(-\frac{4}{3}\pi R^3\ \rho\Delta s_f\ \Delta T + 4\pi R^2\ \gamma_{sl}\right) f(\theta), \quad f(\theta) = \frac{1}{4}(2+\cos\theta)(1-\cos\theta)^2$$

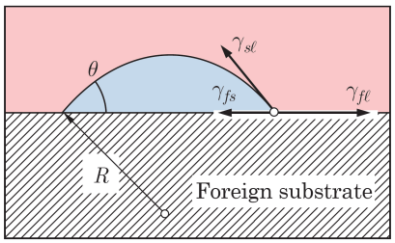

Spherical solid cap of a nucleated embryo of phase s on the surface of a foreign particle present in phase l (Dantzig and Rappaz, Solidification (2016) EPFL Press)

  - The nucleus becomes stable if its size exceed the critical radius R_c defined at the maximum of ΔG,

$$\Delta G_n^{heter} = \Delta G_n^{homo} f(\theta) = \frac{16\pi}{3}\frac{\gamma_{sl}^3}{(\rho\Delta s_f)^2\Delta T^2} f(\theta)$$

  - The nucleation rate is given by $$I^{heter} = \frac{dN(t)}{dt} = (N_p - N(t))\ \nu_0 p_c\ \exp\left(-\frac{16\pi}{3}\frac{\gamma_{sl}^3 f(\theta)}{(\rho\Delta s_f \Delta T)^2 k_B T}\right)$$

    where N_p is the total density of potent particles in phase l corresponding to the wetting angle θ.

MINES PARIS | PSL | Cemef | cnrs

Growth

- Hypotheses
  - Binary alloy of solute compositions x_0
  - Semi-infinite matrix of phase m
  - Spherical precipitate of phase p
  - Constant and equal molar volume in m and p
  - Isothermal system T
  - Constant diffusion in m, D^m
  - Homogeneous composition of the precipitate, $\langle x^p \rangle^p = x^{pm}$

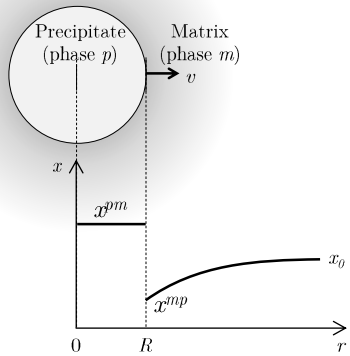

Schematic of composition profile in the matrix m during growth of precipitate p

- Mathematical problem
  - Solute mass conservation in m $$\frac{\partial x^m}{\partial t} = \frac{D^m}{r^2}\frac{\partial}{\partial r}\left(r^2\frac{\partial x^m}{\partial r}\right)$$
  - Solute balance at interface $r = R$ $$v\,(x^{mp} - x^{pm}) = -D^m \left.\frac{\partial x^m}{\partial r}\right|_{pm} + \frac{R}{3}\frac{\partial x^{pm}}{\partial t}$$
  - Thermodynamic equilibrium at R $$x^{mp} = F^{mp}(T,R), \quad x^{pm} = F^{pm}(T,R)$$
  - Condition at infinity when $r \to \infty$ $$\lim_{r\to\infty} x^m(r,t) = x_0$$
  - Initial conditions ($t = 0$ s) $$R = R_0 \approx 0,\ x^m = x_0 \quad \forall r > R_0$$

MINES PARIS | PSL | Cemef | cnrs

Growth (cont'd) — Diffusional phase transformation

- Laplace approximation for a binary alloy (only one solute species) $\frac{D^m}{r^2}\frac{\partial}{\partial r}\left(r^2\frac{\partial x^m}{\partial r}\right)=0$
  - Solution considering the conditions at interface $x^{mp}=F^{mp}(T,R)$ and at infinity $\lim_{r\to\infty}x^m(r,t)=x_0$

$$x^m(r)=R\,\frac{x^{mp}-x_0}{r}+x_0 \quad \forall r>R$$

  - Growth rate (further assuming no flux in the precipitate, $x^{pm}=x^{pm}{}_\infty, \partial x^{pm}/\partial t=0$)

$$v=\frac{D^m}{R}\,\Omega \quad \text{where} \quad \Omega=\frac{x^{mp}-x_0}{x^{mp}-x^{pm}} \quad \text{is the supersaturation of the matrix}$$

  - Time dependence of radius and velocity

$$R=\sqrt{2\,D^m\,\Omega}\,\sqrt{t}$$

$$v=\sqrt{\frac{D^m\,\Omega}{2}}\,\frac{1}{\sqrt{t}}$$

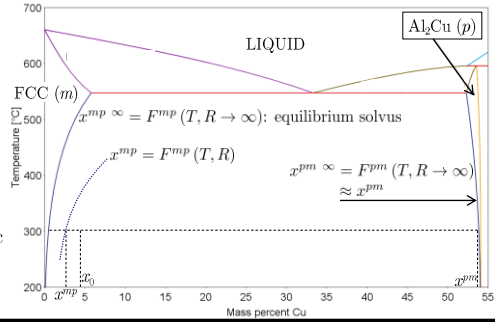

Al – Cu phase diagram and schematic effect of curvature on the solvus temperature of the FCC phase

MINES PARIS | PSL | Cemef | cnrs

33

Growth (cont'd) — Diffusional phase transformation

- Zener solution to the diffusion problem for a binary alloy $\frac{\partial x^m}{\partial t}=\frac{D^m}{r^2}\frac{\partial}{\partial r}\left(r^2\frac{\partial x^m}{\partial r}\right)$

$$\Omega=\frac{\xi}{2}\left(1-\frac{\sqrt{\pi}}{2}\,\sqrt{\xi}\,e^{\xi/4}\,\mathrm{erfc}\left(\frac{\sqrt{\xi}}{2}\right)\right) \quad \text{with} \quad \xi=\frac{2\,R\,v}{D^m}$$

  - The Laplace approximation is retrieved for $\Omega\to 0$
  - The Laplace approximation should only be used for small values of the supersaturation, i.e. small values of $(R\ v\ /\ D^m)$
  - … however the Zener solution does not hold for negative supersaturation (i.e. dissolution)!

Comparison of the growth parameter given by the Laplace approximation with the exact Zener solution as a function of the supersaturation

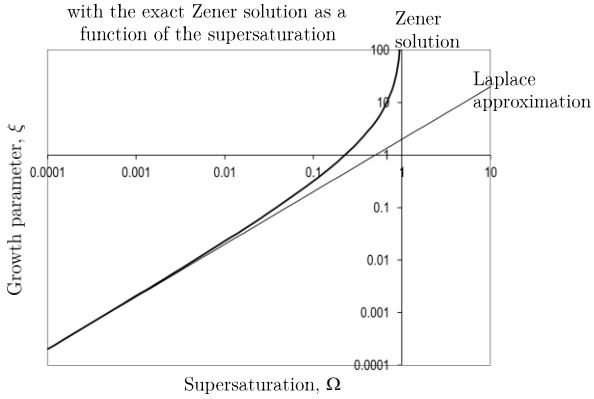

MINES PARIS | PSL | Cemef | cnrs

Zener, journal of applied physics 20 (1949) 950
Aaron et al., journal of applied physics 41 (1970) 4404

34

Coarsening — Diffusive phase transformations

- Origin of the driving force
  - The composition in the matrix phase l at the interface of a particle s depends on its size (curvature effect on thermodynamic equilibrium).
  - Between particles of different size, the difference in composition creates a solute flux at the origin of coarsening or Ostwald ripening or LSW theory.
  - The consequence is an evolution of the microstructure that coarsens.
- Time evolution during coarsening
  - Average size of the particles $\bar{R}^3 = Kt$
  - Log-normal size distribution
  - Constant volume fraction of phase s
  - Global decrease of the surface between phase s and phase l

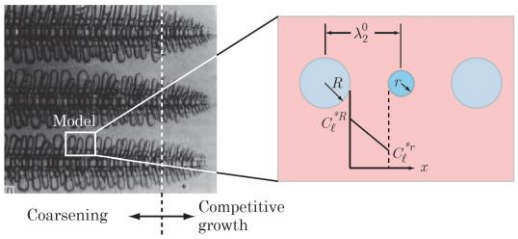

Schematics of the composition gradient between particles of different size leading to coarsening (Dantzig and Rappaz, Solidification (2016) EPFL Press)

Ostwald, zeitschrift für physikalische chemie 37 (1901) 385
Lifshitz, Slyozov, journal of physics and chemistry of solids 19 (1961) 35
Wagner, zeitschrift für elektrochemie 65 (1961) 581

Kinetics of precipitation — Example #2

- Models are developed to concomitantly simulate nucleation, growth and coarsening of precipitates formed in a matrix, solving (equations for the numerical model)
  - Conservation for the density of precipitates, N
  - Growth rate of the precipitates, v
  - Source term for the nucleation of the precipitates, J
  - Solute conservation equation for the system at global composition x_0, precipitate composition $x_p(r)$ and matrix average composition x^m

$$\frac{\partial N}{\partial t} = -\frac{\partial}{\partial r}(N\ v) + J$$

$$v = \frac{D}{r}\ \frac{x^m - x^{mp}}{x^{pm} - x^{mp}}$$

$$J = (N_{max} - N_{tot})\ \beta \exp\left(-\frac{\Delta G^*_{hom}\ f(\theta)}{kT}\right)$$

$$\int_0^\infty \frac{4}{3}\pi r^3\ \frac{\partial N}{\partial r}\ (x^p - x^m)\, dr = x_0 - x^m$$

N_{max}: nucleation density

$N_{tot} = \int_0^\infty \frac{\partial N}{\partial r} dr$: total density

λ: diffusion distance in m

$\beta = 4\pi r^{*2} D x^m / \lambda^4$: rate coefficient

$r^* = (2\gamma V)/\Delta G_n$: critical size nucleus

ΔG_n: driving force for nucleation

$f(\theta)$: wetting function

Langer, Schwartz, physical review A21 (1980) 948
Kampmann, Wagner, Pergamon Press, Oxford (1984) 91

Numerical versus analytical models

Example #2

- Numerical models have left little place for analytical approaches, as they convey the usual advantages
  - Non monotonic size distribution of particles
  - Non isothermal holding
  - Handling of several phases of precipitates
  - Multicomponent alloys
  - Coupling with thermodynamic databases
  - ...

... yet longer simulation times.

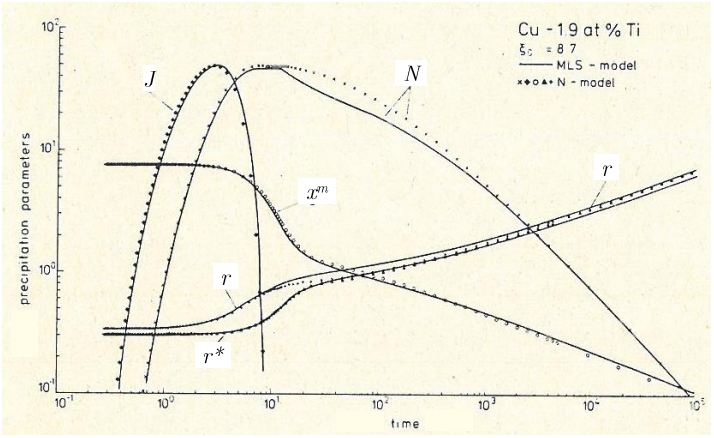

Comparison of precipitation kinetics simulated by analytical and numerical models for a binary alloy under isothermal heat treatment

MINES PARIS | PSL | Cemef | cnrs

Langer, Schwartz, physical review A21 (1980) 948
Kampmann, Wagner, Pergamon Press, Oxford (1984) 91

Precipitation of p-Al_2Cu in m-FCC matrix

Example #2

- Simulation data
- Simulation data
  - Al – 4 wt% Cu
  - $\gamma = 0.2$ J m^{-2}
  - $N_{max} = 10^{22}$ m^{-3}
  - $V^m = 2.1\ 10^{-5}$ m^3 mol^{-1}
  - $D_0 = 0.444\ 10^{-3}$ m^2 s^{-1}
  - $Q = 133900$ J mol^{-1}
  - $\theta = 30$ °
  - $T = 150$ °C

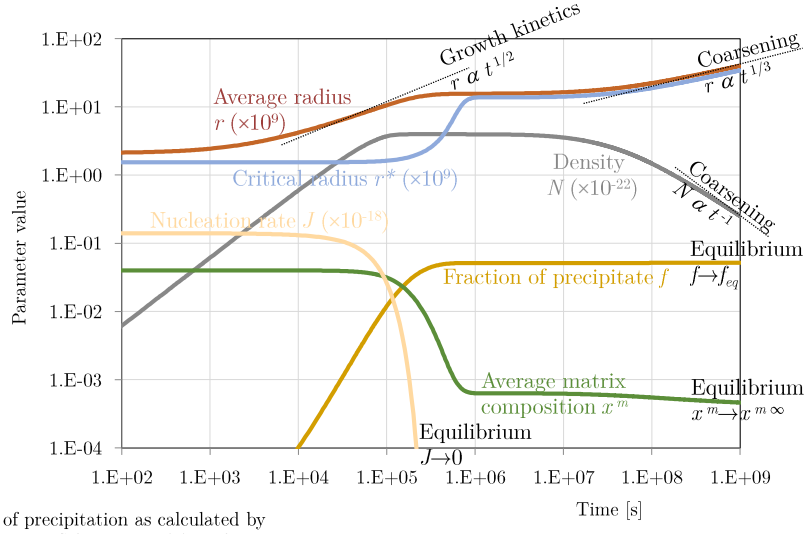

Kinetics of precipitation as calculated by the Langer Schwartz model, with evidence of limit behaviors

MINES PARIS | PSL | Cemef | cnrs

Gandin et al., acta materialia 50 (2002) 901

Observation of precipitation

Example #2

- Samples are analyzed by atom probe tomography for several durations of a given heat treatment
  - Alloy Ni - 6.5 at.% Al - 9.5 at.% Cr
  - Temperature 600 °C
  - Matrix m γ-phase
  - Precipitates p γ'-phase
- Main characterizations of a sample include
  - Redistribution of solutes
  - Shape, size and density of the precipitates
- Several interplaying phenomena are observed
  - Nucleation
  - Growth
  - Coarsening

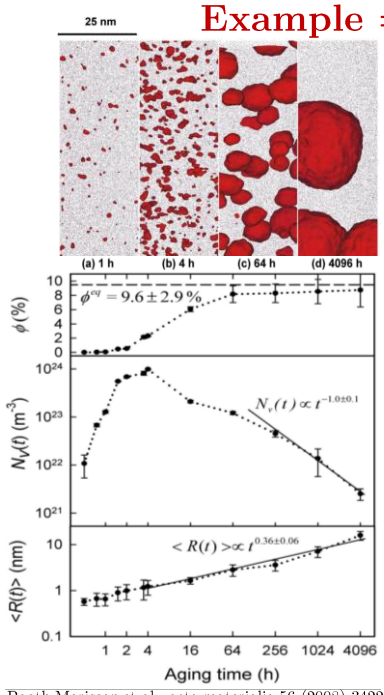

Measured time evolution of the phase fraction, number density and average radius of the precipitates during aging in a nickel-based alloy

Booth-Morisson et al., acta materialia 56 (2008) 3422

Extension of the Zener solution for multicomponent alloys

Example #2

- Hypotheses
  - N solute compositions $\mathbf{x_0} = \{x_{i,0}\}_{1 \le i \le N}$
  - Semi-infinite matrix of phase m
  - Spherical precipitate of phase p
  - Constant and equal molar volume in m and p
  - Isothermal system T
  - Constant diffusion matrix in m, $\mathbf{D}^m = \{D_{ij}^m\}_{1 \le (i,j) \le N}$
  - Homogeneous composition of the precipitate, $\langle x_i^p \rangle^p = x_i^{pm}$
- Mathematical problem $\forall i \in \{0, N\}$
  - Solute mass conservation in m $$\frac{\partial x_i^m}{\partial t} = \sum_{j=1}^{N} \frac{D_{ij}^m}{r^2} \frac{\partial}{\partial r}\left(r^2 \frac{\partial x_j^m}{\partial r}\right)$$
  - Solute balance at interface $r = R$ $$v\,(x_i^{mp} - x_i^{pm}) = -\sum_{j=1}^{N} D_{ij}^m \left.\frac{\partial x_j^m}{\partial r}\right|_{pm} + \frac{R}{3}\frac{\partial x_i^{pm}}{\partial t}$$
  - Thermodynamic equilibrium at R $$x_i^{mp} = F_i^{mp}(T, R), \quad x_i^{pm} = F_i^{pm}(T, R)$$
  - Condition at infinity when $r \to \infty$ $$\lim_{r\to\infty} x_i^m(r,t) = x_{i,0}$$
  - Initial conditions ($t = 0$ s) $$R_0 \approx 0,\ x_i^m = x_{i,0} \quad \forall r > R_0$$

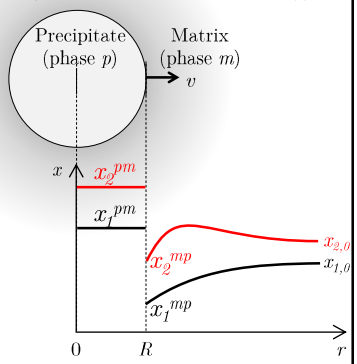

Schematic of composition profile in the matrix m during growth of precipitate p

Guillemot, Gandin, acta materialia 134 (2017) 375

Extension of the Zener solution (cont'd) — Example #2

- Solute profile is a N-linear combination of the solution for the 1-component expression

$$x_i^m = x_{i,0}^m + \sum_{j=1}^{N} K_j U_{ij} F\left(\frac{r^2}{B_j\, t}\right) \quad \text{where} \quad F(u) = \frac{e^{-u/4}}{\sqrt{u}} - \left(\frac{\sqrt{\pi}}{2}\right) \operatorname{erfc}\left(\frac{\sqrt{u}}{2}\right)$$

B_j is the $j-$eigenvalue of matrix $\mathbf{D}^m$
U_{ij} is the $i-$component of the $j-$unitary eignenvector $\mathbf{U}_j$ of matrix $\mathbf{D}^m$
K_j is the $j-$component of vector $\mathbf{K}$ defined below

- A unique solution for the interface position is given by $R^2 = \lambda' t$, where λ' is determined by the N-interfacial solute balances:

$$(\mathbf{x}^{mp} - \mathbf{x}^{pm}) = \mathbf{\Lambda}(\lambda')\,(\mathbf{x}^{mp} - \mathbf{x}_0) \quad \text{where} \quad \Lambda_{ij}(\lambda') = \sum_{k=1}^{N} U_{ik} U_{kj}^{-1} G\left(\frac{\lambda'}{B_k}\right) \text{ and } \quad G(u) = -4\,\frac{F'(u)}{F(u)}$$

- The composition profile is computed from the norm of the eigenvectors, the K_j values being determined by solving

$$\mathbf{K} = \mathbf{\Gamma}(\lambda')\,(\mathbf{x}^{mp} - \mathbf{x}_0) \quad \text{where} \quad \Gamma(\lambda')_{ij} = \frac{U_{ij}^{-1}}{F\,(\lambda'/B_i)}$$

MINES PARIS | PSL | Cemef | cnrs

Guillemot, Gandin, acta materialia 134 (2017) 375 41

Application to Ni – Al – Cr — Example #2

- Physical parameters
  - Thermodynamics database: NI20 — Thermo-Calc
  - Alloy composition $x_{Al,0}$: 7.56 at%
    $x_{Cr,0}$: 8.56 at%
  - Fixed temperature T_0: 600 °C
  - Initial radius R_0: 0 nm
  - Diffusion [$\times 10^{-21}$] $\mathbf{D}^{\gamma}_{cro}$ (Al: 20.8, 8.59; Cr: 8.13, 3.82) $\mathbf{D}^{\gamma}_{inf}$ (20.8, **0**; 8.13, 3.82) $\mathbf{D}^{\gamma}_{sup}$ (20.8, 8.59; **0**, 3.82) $\mathbf{D}^{\gamma}_{dia}$ (20.8, **0**; **0**, 3.82) $m^2\,s^{-1}$
- Numerical model
  - Diffusion [$\times 10^{-19}$] $\mathbf{D}^{\gamma'}$ (Al: 1, 0; Cr: 0, 1) $m^2\,s^{-1}$ — taken artificially large
  - Droplet radius R_f: 100 nm — "semi-infinite" domain
  - Mesh n^{γ}, $n^{\gamma'}$: 500 -
  - Time step Δt: 5 10^{-2} s

MINES PARIS | PSL | Cemef | cnrs

Guillemot, Gandin, acta materialia 134 (2017) 375
Langer et al., acta materialia 60 (2012) 1871 42

Application to Ni – Al – Cr (cont'd)

Example #2

- Simulation with the $\mathbf{D}^{\gamma}_{\mathbf{inf}}$ matrix
- The analytical solution ([A] diamonds symbols) super-imposes on the numerical solution ([N] dotted curves)
- Al depletes / Cr accumulates ahead of the interface
- A typical non monotonous composition profile is found for Cr (cross diffusion effect)
- The numerical model does use a finite matrix, hence deviation from the analytical solution at the outer boundary of the simulation

Validation of the *N*-component analytical solution for the growth of a single precipitate

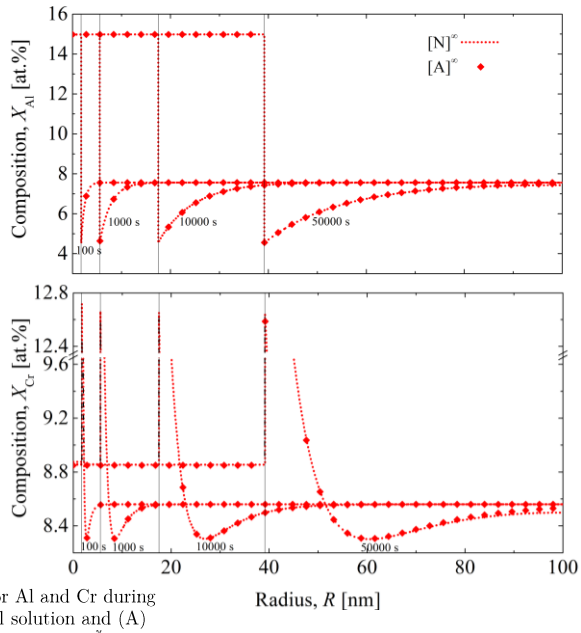

Computed composition profiles at 4 times for Al and Cr during isothermal precipitation with (N) numerical solution and (A) analytical solution using the full diffusion matrix $\mathbf{D}^{\gamma}_{\mathbf{inf}}$

Guillemot, Gandin, acta materialia 134 (2017) 375 43

Application to Ni – Al – Cr (cont'd)

Example #2

- Analytical solution ([A] diamond symbols) superimposes on the numerical solution ([N] dotted curves) for all matrices
- Strong effect of the γ diffusion matrix on the growth velocity of the γ' precipitate
- The selected tie-line depends on $\mathbf{D}^{\gamma}$
- Computation time: [N] 1 h vs. [A] few s

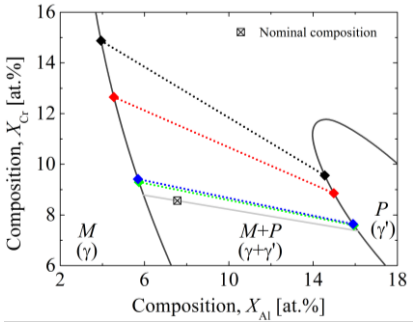

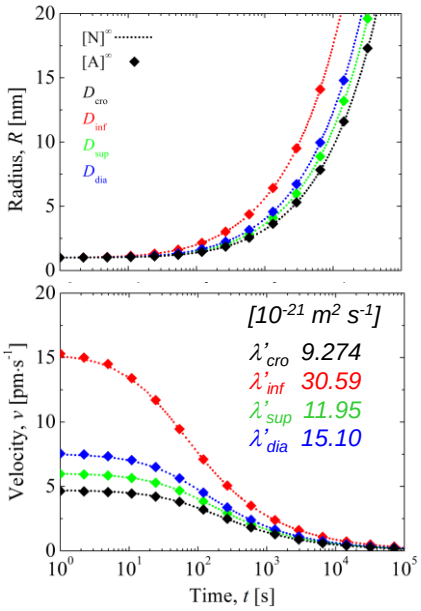

Time evolution of (top right) radius and (bottom right) velocity as a function of the diffusion matrix and (left) corresponding selected tie-line with [N] numerical solution and [A] analytical solution

Guillemot, Gandin, acta materialia 134 (2017) 375 44

Application to Ni – Al – Cr (cont'd)

Example #2

- Comparison with Chen et al. analytical solution [CJA] (open diamond symbols)
  - does not verify the exact solution,
  - is only an approximation that substantially deviates from the exact solution (e.g., $\mathbf{D}^{\gamma}_{\mathbf{cro}}$),
  - is only valid with no interaction between species (i.e., $\mathbf{D}_{\mathbf{dia}}$),
  - provides different λ' growth parameters.

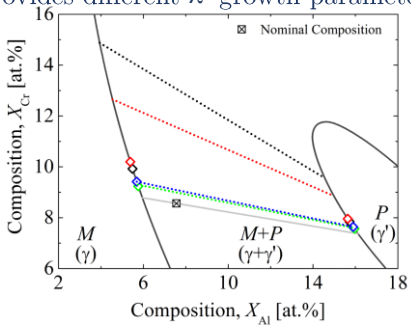

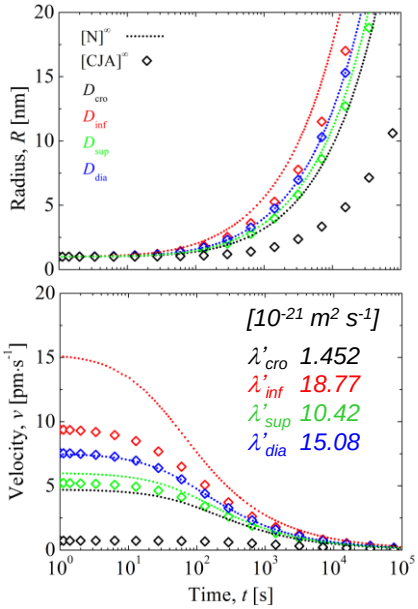

Time evolution of (top right) radius and (bottom right) velocity as a function of the diffusion matrix and (left) corresponding selected tie-line with [A] analytical solution and [CJA] the Chen et al. model.

Chen et al., acta materialia 56 (2008) 1890
Guillemot, Gandin, acta materialia 134 (2017) 375

Example #2

- Interaction with the boundary of the domain (10.6 nm) reflects interaction between precipitates
- The final size (5.7 nm) verifies equilibrium
- An alternate growth/dissolution regime is observed when approaching equilibrium
- Extension of the Laplace approximation for a full diffusion matrix is used for dissolution (as the extended Zener solution is only valid for growth)

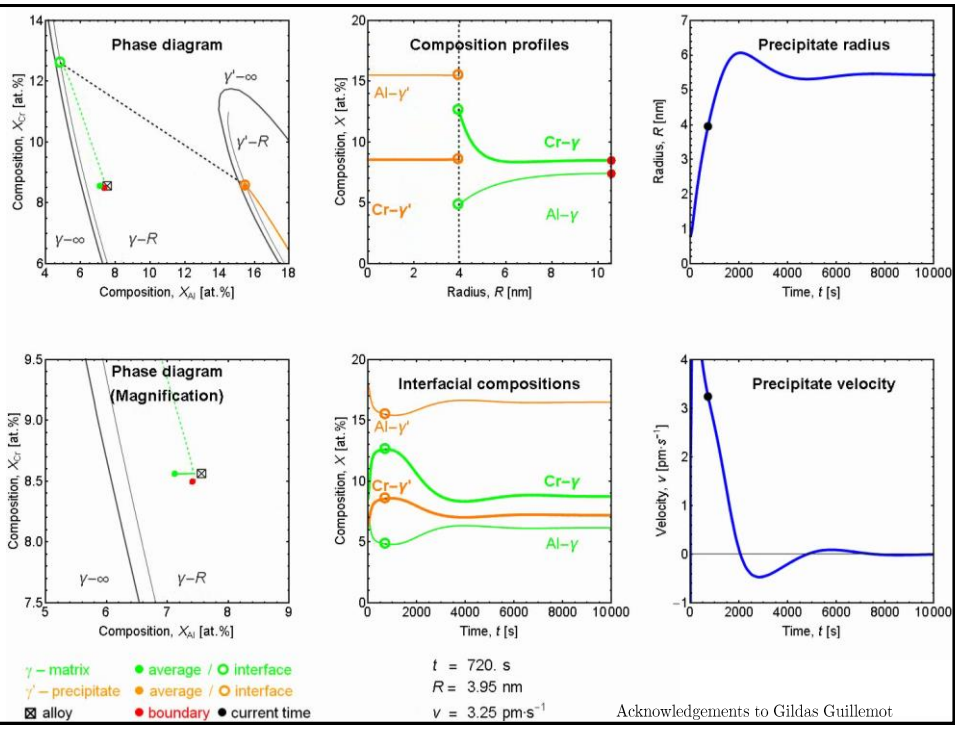

Acknowledgements to Gildas Guillemot

Averaging theorems — Volume averaging

- Objective: solve the conservation equations in all phases at the scale of a small representative volume element (RVE) of volume V

Schematics of a two-phase RVE undergoing transformation

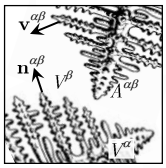

- Definition of average quantities
  - ψ^{φ} quantity in phase $\varphi = \{\alpha, \beta, ...\}$
  - γ^{φ} presence function of phase φ
  - g^{φ} volume fraction of phase φ
  - V^{φ} volume of phase φ

$$\text{Averaging operator: } \langle\psi^{\varphi}\rangle = \frac{1}{V}\int_{V}\gamma^{\varphi}\,\psi\,dV$$

$$\text{Intrinsic average: } \langle\psi^{\varphi}\rangle^{\alpha} = \frac{1}{V^{\varphi}}\int_{V}\gamma^{\varphi}\,\psi\,dV$$

- Averaging theorems at interface $\alpha\beta$
  - $v^{\alpha\beta}$ velocity of interface $\alpha\beta$
  - $A^{\alpha\beta}$ area or interface $\alpha\beta$
  - $\mathbf{n}^{\alpha\beta}$ outwardly directed normal unit vector at interface $\alpha\beta$

$$\text{Time: } \langle\frac{\partial\psi^{\alpha}}{\partial t}\rangle = \frac{\partial\langle\psi^{\alpha}\rangle}{\partial t} - \frac{1}{V}\sum_{\beta(\beta\neq\alpha)}\left(\int_{A^{\alpha\beta}}\psi^{\alpha}\mathbf{v}^{\alpha\beta}\mathbf{n}^{\alpha\beta}dA\right)$$

$$\text{Space: } \langle\nabla\psi^{\alpha}\rangle = \nabla\langle\psi^{\alpha}\rangle + \frac{1}{V}\sum_{\beta(\beta\neq\alpha)}\left(\int_{A^{\alpha\beta}}\psi^{\alpha\beta}\mathbf{n}^{\alpha\beta}dA\right)$$

- Application to the conservation equations (no advection)
  - ρ^{φ} density of phase φ
  - $\mathbf{j}_i^{\varphi}$ diffusive flux of element i in phase φ
  - w_i^{φ} mass fraction of element i in phase φ $\quad i = \{A, B, ...\}$

$$\text{Total mass: } \frac{\partial\rho^{\alpha}}{\partial t} = 0$$

$$\text{Mass of element } i\text{: } \frac{\partial(\rho^{\alpha}w_i^{\alpha})}{\partial t} + \nabla\cdot\mathbf{j}_i^{\alpha} = 0$$

MINES PARIS | PSL | Cemef | cnrs

Averaging theorems (cont'd) — Volume averaging

- Average conservation equations in phase α

$$\text{Total mass: } \frac{\partial\langle\rho^{\alpha}\rangle}{\partial t} = \sum_{\beta(\beta\neq\alpha)}\Gamma^{\alpha\beta} \qquad \text{Mass of element } i\text{: } \frac{\partial\langle\rho^{\alpha}w_i^{\alpha}\rangle}{\partial t} + \nabla\cdot\langle\mathbf{j}_i^{\alpha}\rangle = \sum_{\beta(\beta\neq\alpha)}J_i^{\Gamma(\alpha\beta)} + \sum_{\beta(\beta\neq\alpha)}J_i^{\mathrm{J}(\alpha\beta)}$$

Exchange rate at interface $\alpha\beta$

$\Gamma^{\alpha\beta}$: total mass due to interface velocity $\quad \Gamma^{\alpha\beta} = \frac{1}{V}\int_{A^{\alpha\beta}}\rho^{\alpha}\,\mathbf{v}^{\alpha\beta}\cdot\mathbf{n}^{\alpha\beta}\,dA$

$J_i^{\mathrm{J}(\alpha\beta)}$: the mass fraction of element i due to diffusion $\quad J_i^{\mathrm{J}(\alpha\beta)} = \frac{1}{V}\int_{A^{\alpha\beta}}\mathbf{j}_i^{\alpha}\cdot\mathbf{n}^{\alpha\beta}\,dA$

$J_i^{\Gamma(\alpha\beta)}$: the mass fraction of element i due to interface velocity $\quad J_i^{\Gamma(\alpha\beta)} = \frac{1}{V}\int_{A^{\alpha\beta}}\rho^{\alpha}\,w_i^{\alpha}\,\mathbf{v}^{\alpha\beta}\cdot\mathbf{n}^{\alpha\beta}\,dA$

- Average mass balances at interface $\alpha\beta$

$$\text{Total mass: } \Gamma^{\alpha\beta} + \Gamma^{\beta\alpha} = 0 \qquad \text{Mass of element } i\text{: } J_i^{\Gamma(\alpha\beta)} + J_i^{\mathrm{J}(\alpha\beta)} + J_i^{\Gamma(\beta\alpha)} + J_i^{\mathrm{J}(\beta\alpha)} = 0$$

MINES PARIS | PSL | Cemef | cnrs

Electromagnetic levitation and atomization — Example #3

- Metallographic observation of gas atomized Ni – 75 at% (58 wt%) Al particles
  - The phase diagram predicts that only the Al_3Ni phase is present
  - Instead, 3 phases are observed: Al_3Ni_2, Al_3Ni, and Al (simplified denomination of the phases)

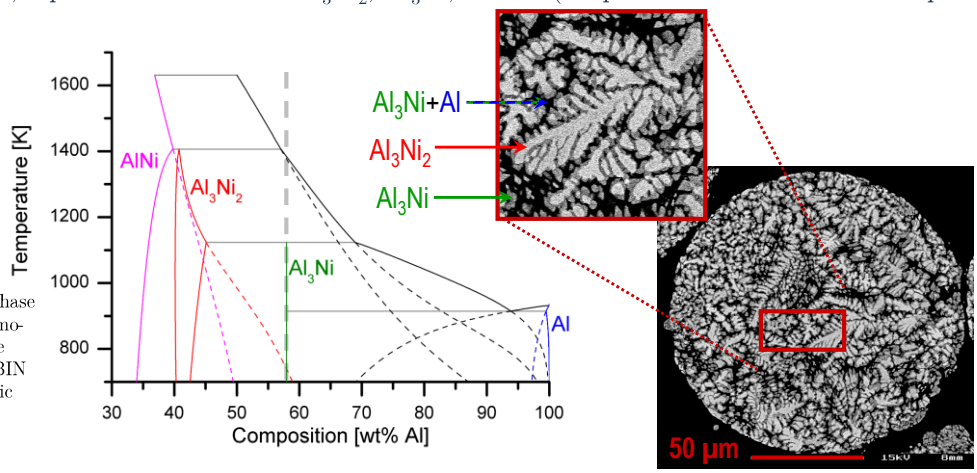

Ni – Al binary phase diagram (Thermo-Calc software calculations, PBIN thermodynamic database)

SEM image of a Ni – 75 at% Al ≈130 µm diameter particle produced by gas atomization

MINES PARIS | PSL | Cemef | cnrs

Tourret et al., acta materialia 59 (2011) 6658 49

Levitated droplet as a model system — Example #3

- Containerless processing of a small levitated droplet
  - Ni – 75 at% Al, droplet mass 890.7 mg
  - Processing under high purity inert gas (He)
  - Temperature recorded by a pyrometer pointing at the sample surface

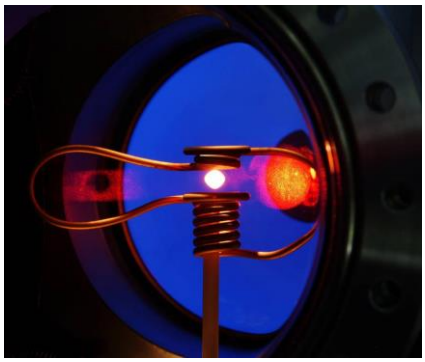

Photography of the electromagnetic levitator and a levitating sample at DLR, Cologne, DE

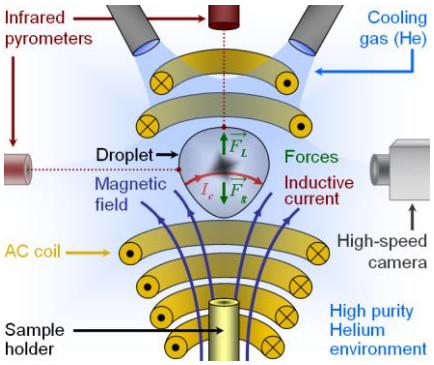

Schematics of the apparatus for electromagnetic levitation

MINES PARIS | PSL | Cemef | cnrs

50

Levitated droplet as a model system (cont'd) — Example #3

- Calibration of the pyrometer
  - Use melting signal and equilibrium temperatures
  - Defines several temperature ranges for calibrations (around liquidus, peritectic, eutectic)
  - Piecewise reconstruction of the cooling curve

Pyrometer calibration procedure showing (black) the raw data and (color) the calibrations defined by temperature intervals

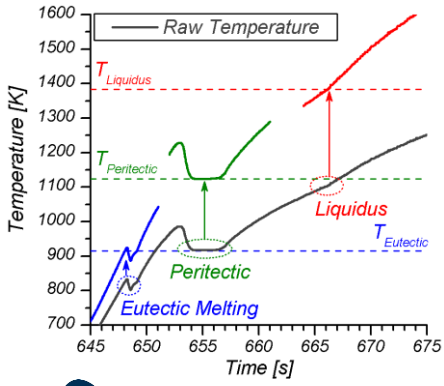

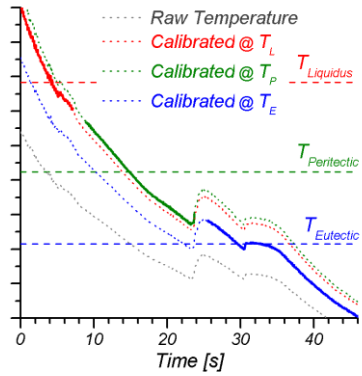

Application of the calibrations to recompose the cooling history from (black) the raw signal

MINES PARIS | PSL | Cemef | cnrs

Tourret et al., acta materialia 59 (2011) 4665 51

Levitated droplet as a model system (cont'd) — Example #3

- Metallography
  - Assembly of high resolution images taken in a central cross section of the solidified droplet collected by scanning electron microscope (SEM)
  - Image processing with multi thresholding
    - phase fractions $g^{Al_3Ni_2}$, g^{Al_3Ni} and $g^{Eutectic}$ (eutectic = Al_3Ni+Al)
    - secondary dendrite arm spacing, λ_2.

High resolution image and its assembly to compose an image of the whole central cross section of the solidified droplet

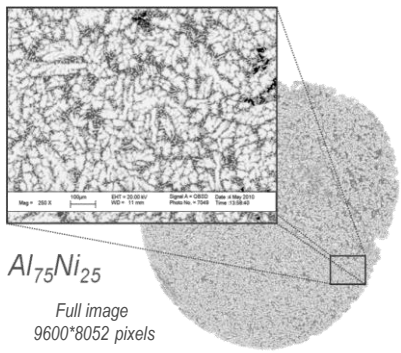

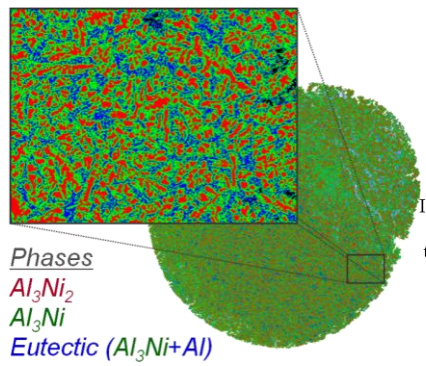

Image analysis with multi thresholding to evaluate the global amount of the phases present in the solidified sample

MINES PARIS | PSL | Cemef | cnrs

Tourret et al., acta materialia 59 (2011) 4665 52

Multiple phase model

Example #3

- Uniform temperature, T
- Heat extraction rate, $\dot{Q} = h_{ext}\ (T - T_{ext})$
  - Constant heat transfer coefficient, h_{ext}
  - Constant gas temperature, T_{ext}
- Constant and equal phase densities, ρ
- Thermodynamic equilibrium at interfaces
- Phases and associated variables

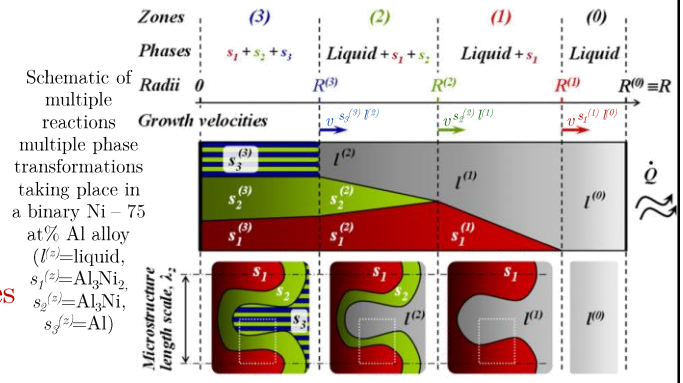

Schematic of multiple reactions multiple phase transformations taking place in a binary Ni – 75 at% Al alloy ($l^{(z)}$=liquid, $s_1^{(z)}$=Al_3Ni_2, $s_2^{(z)}$=Al_3Ni, $s_3^{(z)}$=Al)

Zones *(z)*	Phases	Microst. kinetics	Interface velocity	Interface composition	Average composition	Average enthalpy ...
liquid *(0)*	$l^{(0)}$				$<w^{l^{(0)}}>^{l^{(0)}}$	$<h^{l^{(0)}}>^{l^{(0)}}$
dendritic *(1)*	$s_1^{(1)}\, l^{(1)}$	$v^{s_1^{(1)}l^{(0)}}$	$v^{s_1^{(1)}l^{(1)}}$	$w^{s_1^{(1)}l^{(1)}}$	$<w^{s_1^{(1)}}>^{s_1^{(1)}}$ $<w^{l^{(1)}}>^{l^{(1)}}$	$<h^{s_1^{(1)}}>^{s_1^{(1)}}$ ...
peritectic *(2)*	$s_1^{(2)}\, s_2^{(2)}\, l^{(2)}$	$v^{s_2^{(2)}l^{(1)}}$	$v^{s_2^{(2)}l^{(2)}}\ v^{s_1^{(2)}s_2^{(2)}}$	$w^{s_2^{(2)}l^{(2)}}\ w^{s_1^{(2)}s_2^{(2)}}$	$<w^{s_1^{(2)}}>^{s_1^{(2)}}$ $<w^{s_2^{(2)}}>^{s_2^{(2)}}$ $<w^{l^{(2)}}>^{l^{(2)}}$	...
eutectic *(3)*	$s_1^{(3)}\, s_2^{(3)}\, s_3^{(3)}$	$v^{s_3^{(3)}l^{(2)}}$	inactive	inactive	$<w^{s_1^{(3)}}>^{s_1^{(3)}}$ $<w^{s_2^{(3)}}>^{s_2^{(3)}}$ $<w^{s_3^{(3)}}>^{s_3^{(3)}}$	...

MINES PARIS | PSL | Cemef | cnrs

Tourret et al., acta materialia 59 (2011) 4665 **53**

Volume averaging for the multiple phase model

Example #3

- Averaged total mass conservation in phase $\alpha = \left\{l^{(0)}, s_1^{(1)}, l^{(1)}, s_1^{(2)}, s_2^{(2)}, l^{(2)}, s_1^{(3)}, s_2^{(3)}, s_3^{(3)}\right\}$
  - in phase α $\dfrac{\partial g^\alpha}{\partial t} = \sum_{\beta(\beta\neq\alpha)} S^{\alpha\beta}\, v_n^{\alpha\beta}$
  - at interface $\alpha\beta$ $v_n^{\alpha\beta} + v_n^{\beta\alpha} = 0$
- Averaged solute mass conservation
  - in phase α $g^\alpha \dfrac{\partial \langle w^\alpha\rangle^\alpha}{\partial t} = \sum_{\beta(\beta\neq\alpha)} \left[S^{\alpha\beta} \left(w^{\alpha\beta} - \langle w^\alpha\rangle^\alpha\right) \left(v_n^{\alpha\beta} + \dfrac{D^\alpha}{l^{\alpha\beta}}\right)\right]$
  - at interface $\alpha\beta$ $\left(w^{\alpha\beta} - w^{\beta\alpha}\right) v_n^{\alpha\beta} + \dfrac{D^\alpha}{l^{\alpha\beta}}\left(w^{\alpha\beta} - \langle w^\alpha\rangle^\alpha\right) + \dfrac{D^\beta}{l^{\beta\alpha}}\left(w^{\beta\alpha} - \langle w^\beta\rangle^\beta\right) = 0$
- Averaged energy conservation

$$\rho \frac{\partial \langle h\rangle}{\partial t} = \rho \sum_\alpha \left(\langle h^\alpha\rangle^\alpha \frac{\partial \langle g^\alpha\rangle}{\partial t} + g^\alpha \frac{\partial \langle h^\alpha\rangle^\alpha}{\partial T} \frac{\partial T}{\partial t} + g^\alpha \frac{\partial \langle h^\alpha\rangle^\alpha}{\partial \langle w^\alpha\rangle^\alpha} \frac{\partial \langle w^\alpha\rangle^\alpha}{\partial t}\right) = -h_{ext}\, S^{ext}\, (T - T_{ext})$$

Geometry & assumption for composition profiles
Boundary conditions
Data
Thermodynamic data

Solute balance
Growth kinetics
Solute balance and continuity
Main unknowns

MINES PARIS | PSL | Cemef | cnrs

Tourret et al., acta materialia 59 (2011) 4665 **54**

Volume averaging for the multiple phase model

Example #3

	$S^{\alpha\beta} = A^{\alpha\beta}/V$ Specific surfaces	$l^{\alpha\beta} = -(w^{\alpha\beta} - \langle w^{\alpha}\rangle^{\alpha}) \Big/ \left.\frac{\partial w^{\alpha}}{\partial \mathbf{n}^{\alpha\beta}}\right\|_{\alpha\beta}$ Diffusion lengths assuming quadratic profiles in the solids	
Zone boundaries with spherical growth	$S^{\alpha^{(m)}\alpha^{(n)}} = \frac{g^{\alpha^{(m)}}}{g^{(m)}} \frac{3R^{(n)^2}}{R^3}$	$\alpha^{(m)}$ exists in only one zone (n) adjacent to (m) $l^{\alpha^{(m)}\alpha^{(n)}} = (R^{(m)} - R^{(p)})/3$	$\alpha^{(m)}$ exists in both neighboring zones (m) $l^{\alpha^{(m)}\alpha^{(n)}} = (R^{(m)} - R^{(p)})/6$
Phase interfaces with plate like geometries	$S^{\alpha^{(m)}\beta^{(m)}} = g^{(m)} \frac{2}{\lambda_2}$	$\alpha^{(m)}$ is in contact with only one other phase $\beta^{(m)}$ $l^{\alpha^{(m)}\beta^{(m)}} = \frac{1}{3} \frac{g^{\alpha^{(m)}}}{g^{(m)}} \frac{\lambda_2}{2}$	$\alpha^{(m)}$ is surrounded by two other phases in zone (m) $l^{\alpha^{(m)}\beta^{(m)}} = \frac{1}{6} \frac{g^{\alpha^{(m)}}}{g^{(m)}} \frac{\lambda_2}{2}$

Diffusion length in the liquid (quasi-stationary diffusion profile in front of a spherical moving boundary)

$$l^{(m)(n)} = \frac{R_i}{Pe_e^3 - Pe_i^3}\left[Pe_e^3 - Pe_i^2 - Pe_i - Iv(Pe_i)Pe_e^3 - \left(Pe_e^2 - Pe_e - 1 - Iv(Pe_e)Pe_e^2\right)\frac{e^{-Pe_e}}{e^{-Pe_i}}Pe_i\right]$$

$Pe_i = R_i v_i / D^l$ and $Pe_e = R_e v_i / D^l$ with moving radius R_i and fixed radius R_e

MINES PARIS | PSL | Cemef | cnrs

Tourret et al., acta materialia 59 (2011) 4665
Martorano et al., metallurgical and materials transactions 34A (2003) 1657

Levitated droplet simulation

Example #3

- Simulation for the Ni - 75 at% Al droplet
  - Database — PBIN
  - System radius [M] — $3.82 \cdot 10^{-3}$ m
  - Dendrite arm spacing [M] — $36 \cdot 10^{-6}$ m
  - Diffusion coefficients
    - Liquid — 10^{-9} m^2 s^{-1}
    - Al_3Ni_2, Al_3Ni — $5 \cdot 10^{-11}$ m^2 s^{-1}
  - Gibbs-Thomson coefficients
    - Al_3Ni_2 — $2 \cdot 10^{-8}$ K m
    - Al_3Ni [M] — $3.5 \cdot 10^{-8}$ K m
    - Al [M] — $1.86 \cdot 10^{-7}$ K m
  - Nucleation undercooling
    - Al_3Ni_2, Al_3Ni, Al [M] — 0 K, 150 K, 15 K
  - Heat transfer [M] — 213.8 W m^{-2} K^{-1}
  - External temperature [M] — 293 K

[M]: deduced from measurements
[M]: Marasli, Hunt, acta materialia (1996)

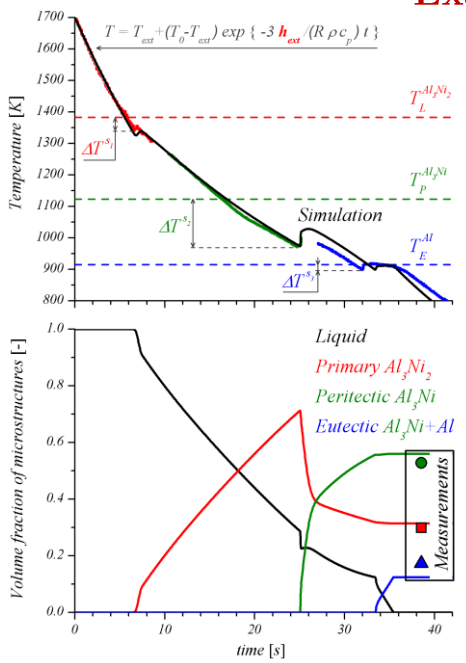

Temperature evolution (black) simulated by volume averaging compared with (colors) measurements

Evolution of phase fraction during the sequence of reactions and transformations and (symbols) measurements

MINES PARIS | PSL | Cemef | cnrs

Tourret et al., acta materialia 59 (2011) 4665

Calibrated model for atomization

Example #3

- Distribution of phases deduced from neutron diffraction analyses (ILL, Grenoble, FR)
- Adaptation from the parameters of the model levitated droplet system
  - No nucleation undercooling
    A new phase s_{i+1} nucleates at the metastable liquidus temperature defined by $T_L^{s_{i+1}}\langle w^{l(i)}\rangle^{l(i)}$
  - Heat transfer $h_{ext}(D, v_D, \kappa_{Ar}, \mu_{Ar}, \rho_{Ar}, B, m)$
    Convective gas flow at the boundary of the particle of diameter D and velocity v_D, with physical properties of the gas and coefficient B and m for a modified Whitaker correlation
  - Microstructure size (λ_2) from SEM analyses
    Linear increase of the DAS with the diameter

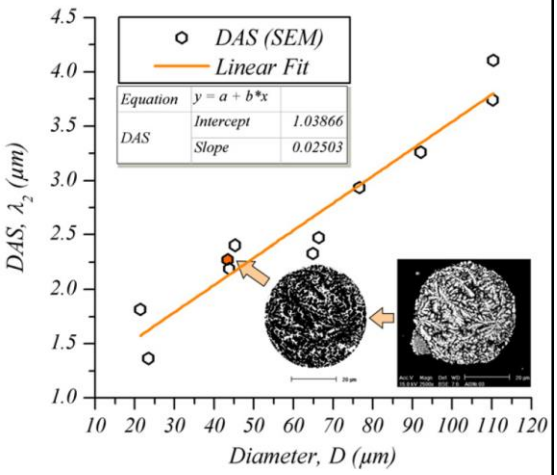

Metallographic inspection of Ni – 75 at% Al particles by SEM revealing the dendrite arm spacing, λ_2, as a function of the diameter of particle produced by gas atomization with argon

Prasad et. al., ISIJ International 49 (2009) 992 57

Calibrated model for atomization (cont'd)

Example #3

- Comparison with atomized droplets
  - *Regime I* *Classical Fourier number analysis*
    The peritectic transformation controls the phase fractions due to diffusion in the solid phases. It is favored for lower cooling rates (larger particles).
  - *Regime III* *Al_3Ni primary growth*
    Primary growth of Al_3Ni controls the phase fraction. It prevents the development of Al_3Ni_2.
  - *Regime II* *Al_3Ni_2 and Al_3Ni growth competition*
    Mixed regime where the peritectic reaction for Al_3Ni can catch-up with the dendritic reaction of Al_3Ni_2 and become primary when the cooling rate is increased.
- Evidence of growth competition between phases formed from the melt

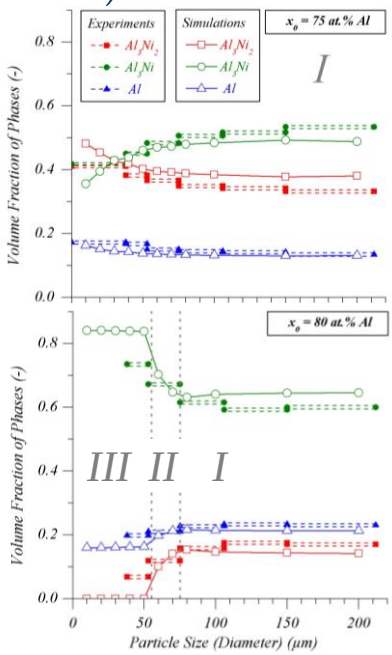

Phase fractions (filled symbols) simulated and (open symbols) measured in atomized Ni – 75 at% Al under Ar gas

Phase fractions (filled symbols) simulated and (open symbols) measured in atomized Ni – 80 at% Al under Ar gas

Tourret et al., acta materialia 59 (2011) 6658 58

Calibrated model for atomization (Cont'd)

Example #3

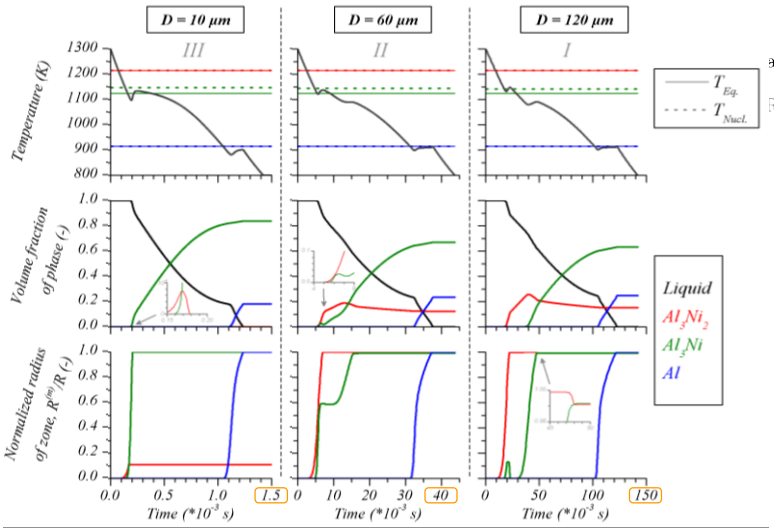

Time evolution of temperature, phase fractions and zone radius during atomization of Ni – 80 at% Al under Ar gas simulated by the volume averaging model. Phase competition is detailed in Regime I (Classical Fourier number analysis), Regime II (Al_3Ni_2 and Al_3Ni growth competition), Regime III (Al_3Ni primary growth).

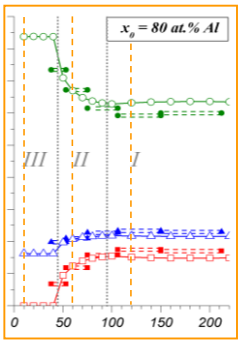

MINES PARIS | PSL | Cemef | cnrs

Tourret et al., acta materialia 59 (2011) 6658 59

@interface

Non-equilibrium phenomena

- Solute trapping
  - When increasing interface velocity v, solute atoms do not have time to escape from the moving interface. The are trapped by the growing phase.
  - This is quantified by $Pe_\delta = v \,/\, v^D$ where $v^D = D^l/\delta$ is the **trans-interface diffusion speed** of atoms through interface thickness δ.
  - For $Pe_\delta >> 1$, full solute trapping occurs, $X_{Bs} = X_{Bl}$, corresponding to temperature $T_0(X_{B0})$, $G_l^m(X_{B0},T_0) = G_s^m(X_{B0},T_0)$ and $\mu_{Bs} \neq \mu_{Bl}$.
- Attachment kinetics
  - It defines the propensity of the atoms of the mother phase to reorganize and join the crystal of the growing phase.
  - A **maximum crystallization speed**, v_0, exists. For $v > v_0$, a glass structure may form.

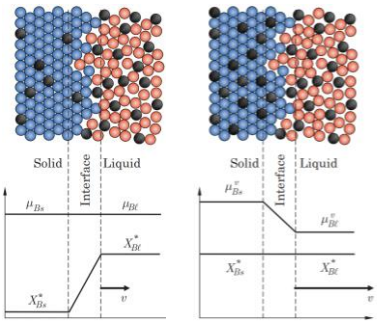

Redistribution of solute at a growing interface (left) under thermodynamic equilibrium, $X_{Bs}<X_{Bl}$, and (right) far from equilibrium, $X_{Bs}=X_{Bl}$ (Dantzig and Rappaz, Solidification (2016) EPFL Press)

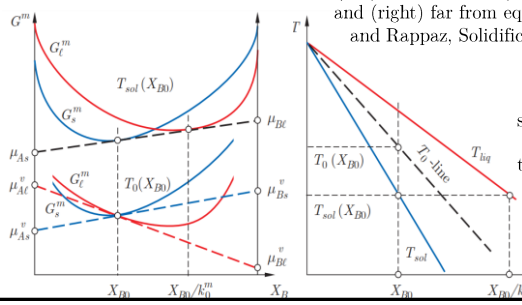

Gibbs free energies for an alloy of composition X_{B0} solidifying under equilibrium conditions at the solidus temperature $T_{sol}(X_{B0})$ and at high speed when complete solute trapping is occurring at $T_0(X_{B0})$ with $G_l^m(X_{B0},T_0)=G_s^m(X_{B0},T_0)$.

MINES PARIS | PSL | Cemef | cnrs

60

@interface (cont'd)

Non-equilibrium phenomena

- Partial solute drag

Materials is adsorbed at composition $x^{eff} \neq x^{\beta}$

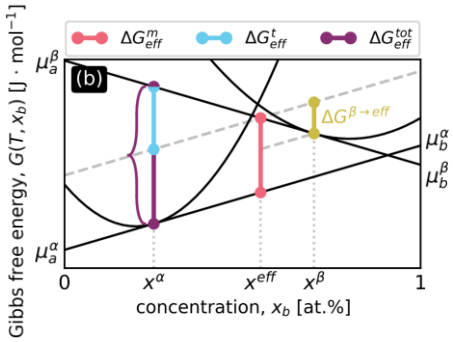

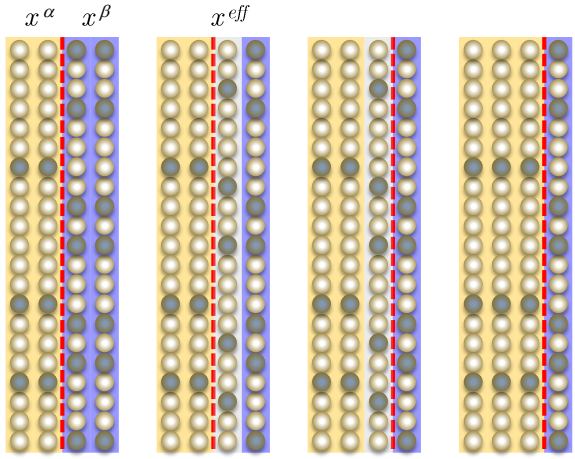

$\Delta G^{\beta \to eff}$
Concentration adjustment

ΔG^m_{eff}
Interface migration

ΔG^t_{eff}
Trans-interface diffusion

ΔG^{tot}_{eff}
Total Gibbs energy dissipation

MINES PARIS | PSL | Cemef | cnrs

Energy dissipation

Non-equilibrium phenomena

- Solidification model with non-equilibrium phenomena @interface
  - Definition of an « effective concentration » of the material adsorbing to the interface

$$x_i^{eff} = \lambda\, x_i^l + (1-\lambda)\, x_i^s \quad \forall\, i \in \{1 : N-1\}$$

λ: solute-drag parameter

  - The energy dissipation associated to the interface migration and trans-interface diffusion leads to

Velocity Response Function (VRF)

$$v = \frac{v_0}{RT} \sum_{i=1}^{N} x_i^{eff} [\![\mu_i]\!] \quad \text{with } [\![\mu_i]\!] = \mu_i^l - \mu_i^s$$

Concentration Response Function (CRF) for solute i

$$v \left(x_i^{eff} - x_i^s \right) = \frac{x_i^{eff} v^D}{RT} \left(\sum_{j=1}^{N} x_j^{eff} [\![\mu_j]\!] - [\![\mu_i]\!] \right) \quad \forall\, i \in \{1 : N-1\}$$

- *A v – dependent T_0 temperature is redefined by explicitly stating $x_i^s = x_i^l\ (= x_i^{eff})$*

$$T_0 = \frac{v_0}{R\, v} \sum_{i=1}^{N} x_i^s (\mu_i^l - \mu_i^s)$$

MINES PARIS | PSL | Cemef | cnrs

Hareland et al., acta materialia 241 (2022) 118407
Martin et al., acta materialia 263 (2024) 119473

Binary multiple phase system (cont'd)

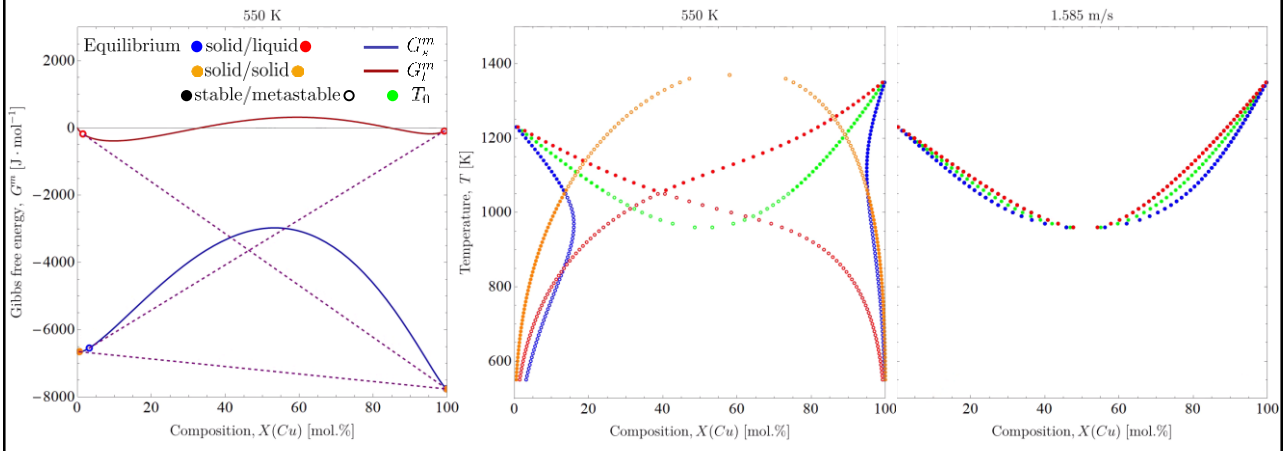

Construction of (center) stable and metastable phase diagram boundaries for the Ag – Cu system from (left) the Gibbs free energy curves, and (right) velocity-dependent (red) kinetics phase diagram ($\lambda = 0.5$, $v^D = 0.4$ m s^{-1}, $v_0 = 850$ m s^{-1}). (red symbols) liquidus, (blue symbols) solidus, (green symbols) T_0, (orange symbols) solvus.

$$G_m^\phi = G_{Ag}^{0,\phi} X_{Ag} + G_{Cu}^{0,\phi} X_{Cu}^\phi + RT\left[X_{Ag}^\phi \ln\left(X_{Ag}^\phi\right) + X_{Cu}^\phi \ln\left(X_{Cu}^\phi\right)\right] + f^\phi X_{Ag}^\phi X_{Cu}^\phi + g^\phi X_{Ag}^\phi X_{Cu}^\phi (X_{Ag}^\phi - X_{Cu}^\phi)$$

ϕ	Liquid	Solid (FCC)
G_{Ag}^0	0	$-11945 + 9.67\,T$
G_{Cu}^0	0	$-13054 + 9.62\,T$
f	$15171 - 2.537\,T$	$34532 - 9.178\,T$
g	$-2425 + 0.946\,T$	$-5996 + 1.725\,T$

Murray, metallurgical transactions 15A (1984) 261, animation provided by Gildas Guillemot

Kinetics phase diagram boundaries (cont'd)

- Multicomponent phase diagram boundaries
  - Solving the VRF and CRFs equations is based on chemical potentials read from thermodynamic database to compute v – dependent properties
    - liquidus temperature, $T_L(v)$,
    - solidus temperature, $T_S(v)$,
    - T_0 temperature, $T_0(v)$,
    - compositions of the phase diagram boundaries, $x_i^s(v)$ and $x_i^l(v)$,
    - segregation coefficients, $k_i^{s/l}(v)$,
    - slopes of the liquidus temperature, $m_i^{s/l}(v)$.
- Limits
  - For $v \to 0$, $T_L(v) \to {}^eT_L$ and $T_S(v) \to {}^eT_S$
  - For high v, $T_L(v) \to T_0$ and $T_S(v) \to T_0$ ($\lambda \neq 0$, $v^D/v_0 << 1$)

IN718 Ni base alloy
$w_{Cr} = 18.2$ wt% $w_{Mo} = 3.1$ wt%
$w_{Fe} = 18.9$ wt% $w_{Ti} = 0.9$ wt%
$w_{Nb} = 5.1$ wt% $w_{Al} = 0.29$ wt% $w_C = 0.025$ wt%
$v_0 = 850$ m · s^{-1}
$v^D = 0.4$ m · s^{-1}
TCNI10 database

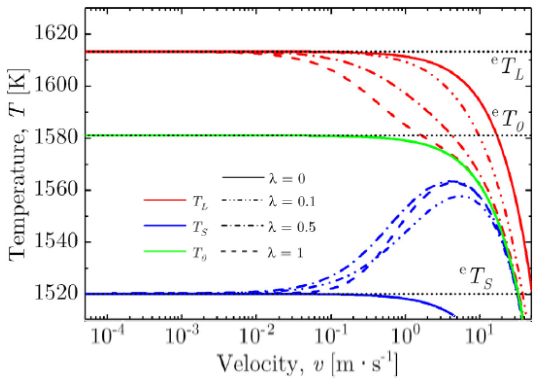

Velocity dependent (red) liquidus, (blue) solidus, (green) T_0 temperatures as a function of velocity and the solute-drag parameter

Martin et al., acta materialia 263 (2024) 119473

Dendrite tip kinetics and phase selection — Example #4

- Fish-scale structure in Additively Manufactured (AMed) 316L stainless steel by laser-powder bed fusion

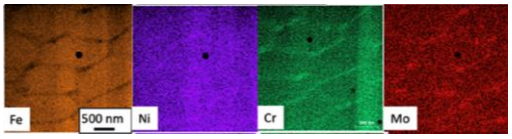

EDS maps in the fish-scale structure region:
interdendritic segregation of Cr and Mo
suggesting γ-austenite solidification

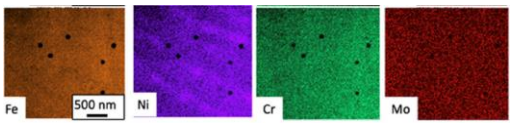

EDS maps outside the fish-scale structure region:
interdendritic segregation of Ni
suggesting δ-ferrite solidification

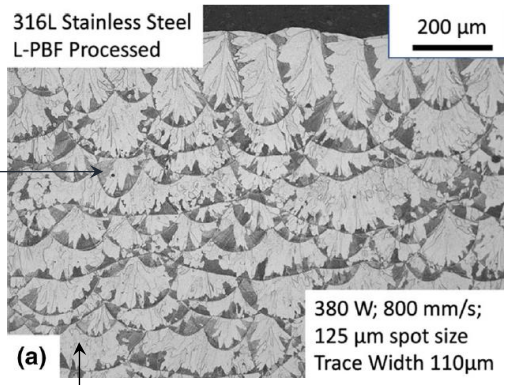

Metallographic cross section transverse to the laser scan showing melt pool boundaries and a fish-scale structure at the boundaries of the melt pool

… the melt pool boundaries in a transverse cross sections solidify with lower velocity !

MINES PARIS | PSL | Cemef | cnrs

Godfrey et al., metallurgical and materials transactions 53A (2022) 3321 65

Dendrite tip kinetics — Example #4

- Interface composition at a paraboloidal dendrite tip of radius r and velocity v

$$x_i^{ls} = x_i^0 + \sum_{j=1}^{N-1}\sum_{k=1}^{N-1} \left(x_k^{ls} - x_k^{sl}\right)\, U_{ij}\, U_{jk}^{-1}\, \mathrm{Iv}(Pe_j)$$

with
- x_i^0 nominal alloy composition for solute species i, $1 \le i \le N-1$
- x_i^{ls}, x_i^{sl} interface composition in the liquid and in the solid, respectively
- Pe_i Peclet number $(rv)/(2B_i)$
- B_i eigenvalue of the diffusion matrix
- $\mathbf{U}_{.,j}$ unit eigenvector of the diffusion matrix
- $\mathrm{Iv}(x)$ Ivantsov function $x\ exp(x)\ \mathrm{E}_1(x)$
- $\mathrm{E}_1(x)$ exponential integral function

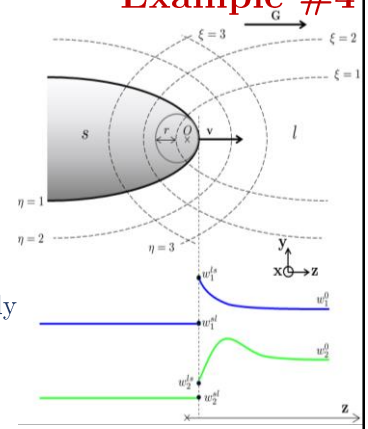

Schematics composition profiles in the liquid l ahead of a paraboloidal dendrite tip of phase s for a multicomponent alloy with solute composition (w_1^0, w_2^0)

MINES PARIS | PSL | Cemef | cnrs

Guillemot et al., CALPHAD 77 (2022) 102429
Hunziker, acta materialia 49 (2001) 4191 66

Dendrite tip kinetics (cont'd) — Example #4

- Stability analysis for a planar front

$$\sum_{i=1}^{N-1} m_i \sum_{j=1}^{N-1} U_{ij} F_j - \Gamma\omega^2 - G = 0$$ where the set of $\mathbf{F} = (F_i)_{1\le i\le N-1}$ coefficients verifies

$$\sum_{j=1}^{N-1}\left[U_{kj}\,\zeta_j - 2\sum_{i=1}^{N-1} U_{ij}\,K_{ki}\right] F_j = -\sum_{j=1}^{N-1} v\,\frac{U_{kj}\,A_j}{B_j}\zeta_j$$

with
- Γ Gibbs-Thomson coefficient
- ω wavenumber of the interface perturbation
- m_i liquidus slope $\left(\partial T/\partial x_i^{ls}\right)\big|_{x_{j\neq i}^{ls}}$
- K_{ij} partition matrix …… $\left(\partial x_i^{sl}/\partial x_j^{ls}\right)\big|_{x_{k\neq j}^{ls}}$
- ζ_i kinetic parameter …… $1-\left(1+(2\omega B_i/v)^2\right)^{1/2}$
- $\mathbf{\Delta x}$ interface composition jump $(x_i^{ls}-x_i^{sl})_{1\le i\le N-1}$
- $\mathbf{A}$ interface composition jump in diagonalized frame $\mathbf{U^{-1}}\cdot\mathbf{\Delta x}$

- Stability criterion with parameter σ

$$(r/\lambda_{min})^2 = \sigma^*/\sigma \quad \text{with} \quad \sigma^* = (2\pi)^{-2}$$

Dendrite tip kinetics (cont'd) — Example #4

- Tip temperature $T_d = \mathrm{F_L}\left(\mathbf{x}^{ls}, \Delta G_\kappa^s, v\right)$

$$\Delta T_d = T_L - T_d = \Delta T_v + \Delta T_\kappa + \Delta T_\chi$$

with
- ΔT_d total undercooling
- ΔT_v kinetic undercooling
- ΔT_κ curvature undercooling
- ΔT_χ chemical undercooling
- T_L liquidus temperature at alloy composition $\mathrm{F_L}\left(\mathbf{x^0}, \Delta G_\kappa^s = 0, v = 0\right)$
- ΔG_κ^s excess Gibbs free energy in the solid phase due to interface curvature
- γ energy of the solid-liquid interface
- V_M^s molar volume of the solid phase $\mathrm{F_{V_M}}\left(\mathbf{x}^{sl}, T\right)$

- Tie line

$$\mathbf{x}^{sl} = \mathrm{F_S}\left(\mathbf{x}^{ls}, \Delta G_\kappa^s, v\right)$$

Phase selection in AMed 316L — Example #4

- Data for simulation of the dendrite tip kinetics

Temperature gradient [K m^{-1}]		G	10^7	Composition [wt%]	Cr 16.81	Ni 11.92	Mo 2.43	Mn 0.99	Si 0.36
Thermodynamic databases		TCFE10 MOBFE5		Diffusion matrix in the liquid at T_L [10^{-9} m^2 s^{-1}]	Cr	Ni	Mo	Mn	Si
BCC_A2	[m s^{-1}]	v_0 (*)	759.	Cr	3.166	0.192	0.670	0.657	0.412
	[m s^{-1}]	v^D (*)	0.72	Ni	0.135	3.400	0.516	-1.097	-3.286
		λ (*)	0.58	Mo	0.056	0.057	2.633	0.017	0.240
	[J m^{-2}]	γ (**)	0.27	Mn	0.045	-0.105	0.006	3.794	-0.157
		σ	$(2\pi)^{-2}$	Si	-0.006	-0.211	0.119	-0.117	3.637
FCC_A1	[m s^{-1}]	v_0 (*)	614.	Cr	3.109	0.195	0.669	0.646	0.424
	[m s^{-1}]	v^D (*)	0.36	Ni	0.135	3.321	0.500	-1.079	-3.235
		λ (*)	0.52	Mo	0.056	0.056	2.584	0.016	0.238
	[J m^{-2}]	γ (**)	0.27	Mn	0.044	-0.104	0.006	3.714	-0.155
		σ	$(2\pi)^{-2}$	Si	-0.005	-0.207	0.117	-0.115	3.562

Godfrey et al., metallurgical and materials transactions 53A (2022) 3321
Martin et al., acta materialia 263 (2024) 119473
(*) Antillon et al., acta materialia 248 (2023) 118769
(**) Jian et al., materials transactions 43 (2002) 721

Phase selection in AMed 316L — Example #4

- The microstructure with the highest temperature is selected
- With temperature gradient 10^7 K m^{-1}, solidification from the liquid is either
  - γ at low and high velocity (planar front at T_S)
  - δ at intermediate velocity
- The partition coefficient reveals
  - segregation of Ni for δ
  - segregation of Mo and Cr for γ

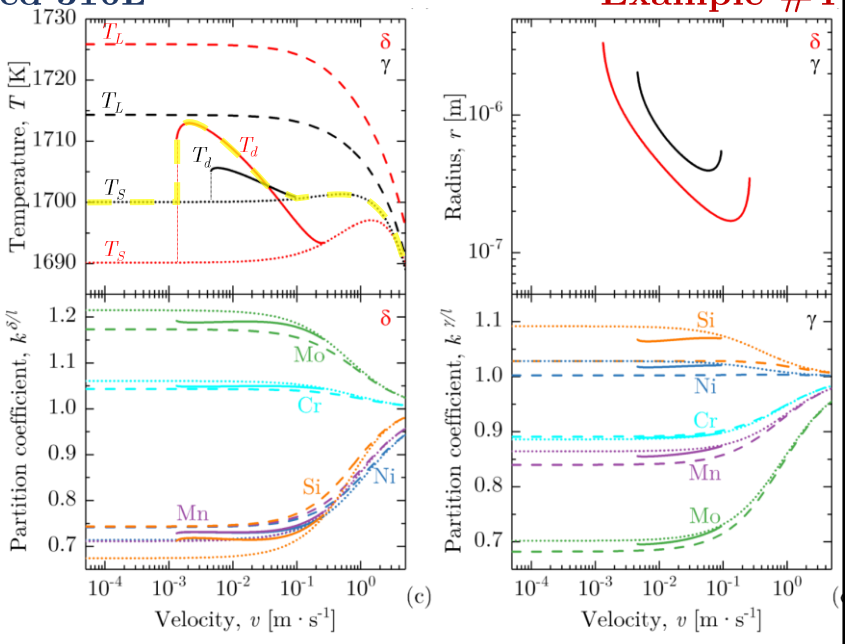

Martin et al., acta materialia 263 (2024) 119473

Phase selection in AMed 316L(cont'd)

Example #4

- The melt pool boundaries in a transverse cross sections solidify with low velocity and high temperature gradient
- For high temperature gradient (10^8 K m^{-1}) and low velocity (<1 mm s^{-1}), γ planar front is favored, growing at the solidus temperature
- For lower temperature gradient (10^7 K m^{-1}) and high velocity (>1 mm s^{-1}), δ is favored, growing at T_d
- The solid in 316L is mainly composed of γ, hence present for epitaxial growth at the melt pool boundaries

γ is shortly selected at the melt pool boundaries, explaining the fish-scale structure

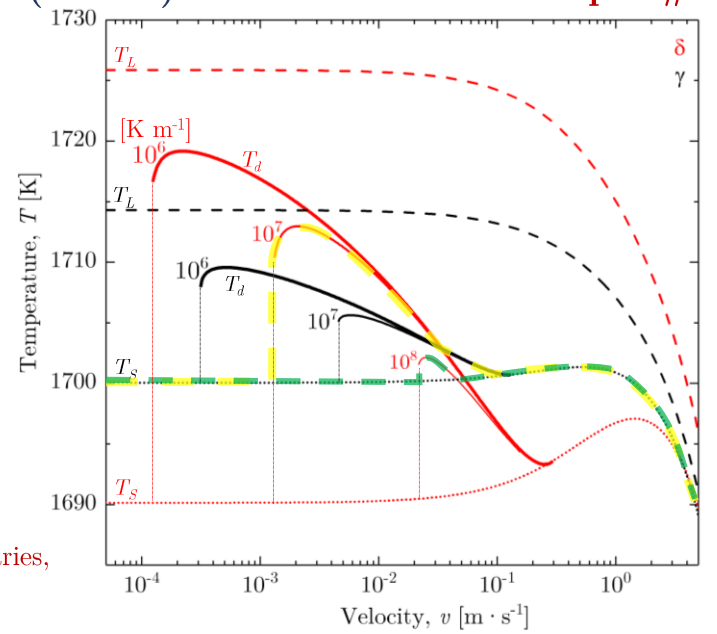

Martin et al., acta materialia 263 (2024) 119473
Godfrey et al., metallurgical and materials transactions 53A (2022) 3321

What we have learned...

Summary

- Thermodynamic
  - How to built an equilibrium phase diagram
  - Application of lever rule transformation paths to the solidification of a binary alloy
- Diffusive phase transformations
  - Effect of curvature and diffusion on nucleation, growth and coarsening
  - Application to precipitation kinetics for multicomponent alloys
- Volume averaging
  - Averaged conservation equations
  - Application to mass and solute mass for the calculation of solidification paths
- Non-equilibrium phenomena
  - Kinetics phase diagram with non-equilibrium phenomena at a phase interface
  - Application to phase selection of microstructures using dendrite tip kinetics

What we have learned... (cont'd) — Summary

- Add-ons
  - Comparison of simulations with
    - experimental data for solidification of a Sn – Pb alloy (collaboration Grenoble INP–UGA, SIMAP/EPM, FR)
    - experimental data for solidification of an Al – Ni levitated droplet (collaboration DLR, Cologne, DE)
    - dendrite tip kinetics for multicomponent alloys (collaboration with Safran Additive Manufacturing Campus, Le Haillan, FR)
  - Animations (G. Guillemot)
    - Growth/dissolution kinetics of a Ni – Al – Cr precipitate
    - Construction of the equilibrium and kinetics Ag – Cu phase diagrams
  - PhysalurgY: physalurgy.cemef.minesparis.psl.eu
    - Kinetic phase diagrams
    - Growth kinetics of dendrites
    - Growth of precipitates

Thank-you! Questions?

MINES PARIS | PSL | Cemef cnrs